Development of a Novel, Manufacturing Method of Producing Cost-Effective Thin-Film Heat Flux Sensors

Rande J. Cherry

Thesis submitted to the faculty of the Virginia Polytechnic Institute and State University in partial fulfillment of the requirements for the degree of

Master of Science

In

Mechanical Engineering

Thomas E. Diller, Co-Chair

Christopher B. Williams, Co-Chair

Khai D. T. Ngo

September 22, 2015

Blacksburg,VA

Keywords: Heat flux measurement, Thin-Film Heat Flux Gage, Heat Flux

Development of a Novel, Manufacturing Method of Producing Cost-Effective Thin-Film Heat Flux Sensors

Rande J. Cherry

Abstract

A new method of manufacturing heat flux sensors was developed using a combination of copper etching and stencil printing nickel/silver conductive ink thermocouple materials onto a thin-film polyimide Kapton® substrate. The semi-automated production capabilities of this manufacturing process significantly decrease the cost of producing thin-film heat flux sensors while still maintaining acceptable performance characteristics. Material testing was performed to first determine the most appropriate materials as well as the theoretical sensitivity and time response of the final sensor. The Seebeck coefficient of a thermocouple formed using the combination of EMS CI-1001 silver and EMS CI-5001 nickel ink was measured to be 18.3 ± 0.9 uV/°C. Calibrations were then performed on a sample of heat flux sensors produced using the novel manufacturing process to verify theoretical values for both sensitivity and time response. The printed heat flux sensor (PHFS) made using this process has a nominal voltage output sensitivity of 4.10 ± 0.23 mV/(W/cm^2) and first order time constant response time of 0.592 ± 0.026 seconds. Lastly, a cost analysis was performed to estimate that the final cost to produce the PHFS is approximately $7.73 per sensor. This cost is significantly lower than commercially available sensors which range from $210 upwards to $3000.

Dedication

This work is dedicated to my parents and family who have given me the opportunities and motivation to stay in school and figure out how much I am truly capable of. To my Dad, your endless knowledge and guidance has been the basis for who I am today. Despite some waivers in self-motivation I think I have proved to you, and myself, that I can keep my nose to the grindstone and do what is necessary to reach my goals. To my Mom, with your love and positive outlook on life you have been a constant inspiration to me. Although I know you would support me in anything I wanted to do, you were the one that first encouraged me to return to school and I can't thank you enough for guiding me to the right decision. My brothers, David and Connor, I thank you for always being there whether I needed advice or just someone to talk to.

Acknowledgments

Dr. Diller, your open door policy and knowledge of heat transfer has been an invaluable resource through the course of my graduate work at Virginia Tech. I've learned an immense amount not only about heat transfer but how to apply my engineering and problem solving skills. I'm glad that you had faith in me joining your lab and I'm lucky to have linked up with you at the beginning of my thesis work.

Dr. Williams, I thank you so much for helping me along the early stages of the engineering design process in developing these sensors. I still remember my freshman year of undergraduate coursework when you would guest speak for the enormous classes to drive in important engineering fundamentals that I still use today.

Dr. Ngo, I appreciate every meeting that we had. Whenever I requested it, you would make yourself available to talk to me and share your knowledge of electronics. Your guidance

during these meetings helped set me down the path that allowed me to design the manufacturing process that I can be proud to present in this paper.

Chris Cirenza, I thank you for all your assistance in developing and building these heat flux sensors. Without your help, the sensors would be nowhere near as developed as they are today. I'm glad that you brought humor and good energy to the lab.

This material is based upon work supported by the National Science Foundation under Grant No. 1254006 under the Transforming Undergraduate Education in Science, Technology, Engineering and Mathematics (TUES) program. Any opinions, findings, and conclusions or recommendations express in this material are those of the authors and do not necessarily reflect the views of the National Science Foundation.

Table of Contents

Abstract ii
Dedication and Acknowledgments iii
Table of Contents v
List of Figures vii
List of Tables viii

Chapter 1: Introduction and Thesis Organization 1
1.1. Introduction 1
1.2. Thesis Organization 1

Chapter 2: Development of a Novel, Manufacturing Method of Producing Cost-Effective Thin-Film Heat Flux Sensors 3
2.1. Abstract 3
2.2. Introduction 3
2.3. Differential-Temperature Heat Flux Sensors 4
2.3.1. Basic Operating Principle 5
2.3.2. Resistance Temperature Detector Based Sensors 6
2.3.3. Thermopile Gages 6
2.4. Design Parameters of Heat Flux Sensors 8
2.4.1. Sensitivity 9
2.4.2. Response Time 9
2.4.3. Thickness and Thermal Resistance 10
2.4.4. Additional Heat Flux Sensor Design Considerations 10
2.5. Commercially Available Thermopile Heat Flux Sensors 11
2.5.1. RDF Corporation Micro-Foil (Version #1) 11
2.5.2. Vatell Episensor 12
2.5.3. BF Heat Flux Transducer 13
2.5.4. Wire Wound Gages 13
2.5.5. Heat Flux Microsensor (HFM) 14
2.5.6. RDF Corporation Micro-Foil (Version #2) 17
2.5.7. Specifications of Commercially Available Heat Flux Sensors 18
2.6. Experimental Construction of PHFS 19
2.6.1. PHFS Design Decisions 19
2.6.2. Copper Etching 21
2.6.3. Laser Drilling Vias 22
2.6.4. Stencil Printing Thermopile Materials 23
2.6.5. Detailed Design of PHFS 24
2.7. Experimental Equipment and Methods 26
2.7.1. Instrumentation 26
2.7.2. Laser Cutting System 27
2.7.3. Seebeck Coefficient Testing Setup 27
2.7.4. Conduction Sensitivity Calibration Setup 28
2.7.5. Radiation Sensitivity Calibration Setup 30
2.7.6. Time Response Experimental Design 31

2.8. Results and Discussion 31
2.8.1. Seebeck Coefficient Results 32
2.8.2. Conduction Sensitivity Calibration Results 33
2.8.3. Radiation Sensitivity Calibration Results 35
2.8.4. Time Response Results 37
2.8.5. Cost Analysis Results 37
2.8.6. Discussion of Results 40
2.9. Conclusions 42
2.10. Acknowledgment 42
2.11. References 42

Chapter 3: Conclusions and Recommendations 45
3.1. Conclusions 45
3.2. Recommendations for Future Work 45

Appendix A: Detailed Manufacturing Process of the PHFS 48
A.1. Preparation of Manufacturing Materials and Equipment 48
A.2. Manufacturing Process of the PHFS 50

Appendix B: Estimation of Uncertainty in Calculations/Measurements 53
B.1. Seebeck Coefficient Uncertainty 53
B.2. Radiation Sensitivity Calibration Uncertainty 54
B.3. Conduction Sensitivity Calibration Uncertainty 56
B.4. Time Response Uncertainty 57

Appendix C: Conduction Sensitivity Calibration Procedure 60
C.1. Necessary Equipment for Conduction Sensitivity Calibration 60
C.2. Conduction Sensitivity Calibration System Hardware Set Up Procedure 60
C.3. Determining Measurement System Voltage Offset 62
C.4. Performing a Conduction Sensitivity Calibration Run 62
C.5. Analyzing the Measured Conduction Sensitivity Calibration Data 63

Appendix D: Radiation Sensitivity Calibration Using Lamp 65
D.1. Necessary Equipment for Radiation Sensitivity Calibration 65
D.2. Experimental Setup for Radiation Sensitivity Calibration 66
D.3. Radiation Sensitivity Calibration Procedure 68
D.4. Radiation Sensitivity Calibration Data Post Processing 69

Appendix E: Programming Code Used for Data Collection/Analysis 71
E.1. MatLab Code Used to Analyze Seebeck Coefficient Data 71
E.2. MatLab Code Used to Analyze Conduction Sensitivity Calibration Data 71
E.3. MatLab Code Used to Analyze Radiation Sensitivity Calibration Data 73

List of Figures

Figure 1.1. Diagram of one-dimensional heat flux through a thermal resistance layer of thickness δ [2]. 5
Figure 1.2. Diagram of the original Micro-Foil heat flux sensor designed by Orlando and Hines and sold by RDF Corporation. 12
Figure 1.3. Diagram of a wire wrapped heat flux sensor. 14
Figure 1.4. Heat flux microsensor gage pattern overlay [13]. 15
Figure 1.5. Diagram of thermocouple junction pairs layout in the second iteration of the heat flux microsensor [14]. 16
Figure 1.6. A partial layout schematic of the RDF Micro-Foil heat flux sensor version #2 17
Figure 1.7. Flowchart of the manufacturing process used to produce the PHFS 20
Figure 1.8. Schematic of the PHFS construction layout for two thermocouple junction pairs 21
Figure 1.9. Picture of the copper trace designs and laser drilled via holes for both the a) top and b) bottom surfaces of the PHFS 22
Figure 1.10. Picture of the PHFS a) top and b) bottom surfaces 25
Figure 1.11. Diagram of the experimental setup used to measure the Seebeck coefficient of a single thermocouple junction 28
Figure 1.12. Diagram of a steady-state conduction sensitivity calibration facility 29
Figure 1.13. Plot of the least squares regression fit model used to determine Seebeck coefficient of the metallic conductive ink thermocouple 32
Figure 1.14. PHFS sensitivities measured using the conduction sensitivity calibration system ..34
Figure 1.15. PHFS voltage output as a function of absorbed heat flux while mounted in the radiation calibration system 36
Figure 1.16. Normalized average PHFS heat flux output voltage as a function of time in response to a step input 37
Figure 1.17. Total cost to manufacture the PHFS as a function of number of sensors in an array during a single manufacturing batch 40
Figure A.1. Dimensioned diagrams of the copper jumper traces on the a) top and b) bottom surfaces of the polyimide Kapton TRL substrate 48
Figure A.2. Dimensioned diagrams of the two printing stencil masks used to pattern the a) silver and b) nickel conductive ink thermopile materials on the top surface of the polyimide Kapton TRL substrate 49
Figure A.3. Dimensioned diagrams of the two printing stencil masks used to pattern the a) silver and b) nickel conductive ink thermopile materials on the bottom surface of the polyimide Kapton TRL substrate 50

List of Tables

Table 1.1. Compiled performance specifications of various heat flux sensors that have been commercially available....18
Table 1.2. Materials required for manufacturing the PHFS....38
Table 1.3. Breakdown of manufacturing steps necessary to produce an array of four PHFS's ..39
Table 1.4. Compiled performance specifications of various heat flux sensors that have been commercially available and the PHFS 41
Table B.1. Uncertainty budget while measuring Seebeck coefficient 54
Table B.2. Uncertainty budget for measuring PHFS sensitivity using the radiation sensitivity calibration system 56
Table B.3. Uncertainty budget for measuring PHFS sensitivity using the conduction sensitivity calibration system 57
Table B.4. Uncertainty budget for PHFS time response measurements....59

Chapter 1: Introduction and Thesis Organization

1.1. Introduction

Heat flux sensors can be used to measure and quantify the thermal energy per unit area moving through a system. They are used by engineers to measure and understand the heat transfer in HVAC systems, insulation analysis, refrigeration systems as well as countless other applications. Although heat flux measurements are extremely valuable in thermal analysis of a system, heat flux sensors are not widely utilized in commercial products and industry testing due to the technology's high retail prices. The motivation of this work is to develop a manufacturing process that will significantly reduce the cost of thin-film heat flux sensors so that they become more readily available.

1.2. Thesis Organization

This thesis consists of three chapters. The second chapter is a journal paper that will be submitted to a heat transfer or scientific measurement technology journal. It explains heat flux sensor operating principals, design considerations as well as current commercially available products. Then it describes the novel manufacturing process that was developed and the resulting performance characteristics of the printed heat flux sensor (PHFS). Chapter 3 is conclusions and recommendations for future work to be performed to further develop the PHFS.

A series of appendices used to support the claims made within the journal paper are also included. Appendix A contains a detailed description of the manufacturing process used to produce a PHFS. Appendix B is a series of calculations used to determine the uncertainty in calculations made from measurements taken during experimental testing. This includes uncertainty in Seebeck coefficient, radiation sensitivity calibrations, conduction sensitivity

calibrations, and time response measurements/calculations. Appendices C and D are detailed procedures used to conduct conduction and radiation sensitivity calibrations respectively. Lastly, Appendix E is a compilation of the Matlab and Labview programs used for data collection and analysis.

Chapter 2: Development of a Novel, Manufacturing Method of Producing Cost-Effective Thin-Film Heat Flux Sensors

Rande J. Cherry, Thomas E. Diller

Department of Mechanical Engineering, Virginia Tech, Blacksburg, VA, 24061, USA

2.1. Abstract

A new method of manufacturing heat flux sensors was developed using a combination of copper etching and stencil printing nickel/silver conductive ink thermocouple materials onto a thin-film polyimide Kapton® substrate. The semi-automated production capabilities of this manufacturing process significantly decrease the cost of producing thin-film heat flux sensors while still maintaining acceptable performance characteristics. Material testing was performed to first determine the most appropriate materials as well as the theoretical sensitivity and time response of the final sensor. The Seebeck coefficient of a thermocouple formed using the combination of EMS CI-1001 silver and EMS CI-5001 nickel ink was measured to be 18.3 ± 0.9 uV/°C. Calibrations were then performed on a sample of heat flux sensors produced using the novel manufacturing process to verify theoretical values for both sensitivity and time response. The printed heat flux sensor (PHFS) made using this process has a nominal voltage output sensitivity of 4.10 ± 0.23 mV/(W/cm^2) and first order time constant response time of 0.592 ± 0.026 seconds. Lastly, a cost analysis was performed to estimate that the final cost to produce the PHFS is approximately $7.73 per sensor. This cost is significantly lower than commercially available sensors which range from $210 upwards to $3000.

2.2. Introduction

During engineering thermal analysis, it is necessary to not only determine the temperature of a position but also the amount of heat or thermal energy being transferred to or

from a system. Heat flux sensors can be used to measure and quantify the thermal energy per unit area moving through a system. They are used to measure and understand the heat transfer in HVAC systems, insulation analysis, refrigeration systems as well as countless other applications. Although heat flux measurements are extremely valuable in thermal analysis of a system, heat flux sensors are not widely utilized in commercial products and industry testing due to the technology's high retail prices.

Thin-film heat flux sensors are desired as measurement devices due to their relatively fast time response and minimal thermal resistance compared to other sensors such as the Schmidt-Boelter gage [1]. Thin-film sensors are also advantageous in convective heat measurement scenarios where a small profile is necessary to minimize boundary layer tripping. Several thin-film heat flux sensors are commercially available but due to certain operating principles of the sensors themselves they must be manufactured using certain manufacturing processes. Currently these processes, such as precision plating, sputtering, copper etching, require a great deal of control and labor that limits manufacturing output and results in high final product costs of at least $250 and upwards to $3000.

2.3. Differential-Temperature Heat Flux Sensors

This section describes the basic operating principles of differential-temperature based heat flux sensors and the different methods of constructing them. Then it discusses the various design parameters and performance characteristics of thermopile sensors. Lastly, it identifies the various commercially available heat flux sensors, their performance characteristics, and stipulated manufacturing methods.

2.3.1. Basic Operating Principle

Differential temperature heat flux sensors function by measuring the temperature difference across a dielectric thermal resistance layer (TRL) substrate. Using Fourier's law of heat conduction with a one-dimensional heat transfer assumption under steady-state conditions, the temperature difference is proportional to the absorbed heat flux

$$q" = -k\,\frac{dT}{dx} = -\frac{k}{\delta}\,(T_2 - T_1) \tag{1.1}$$

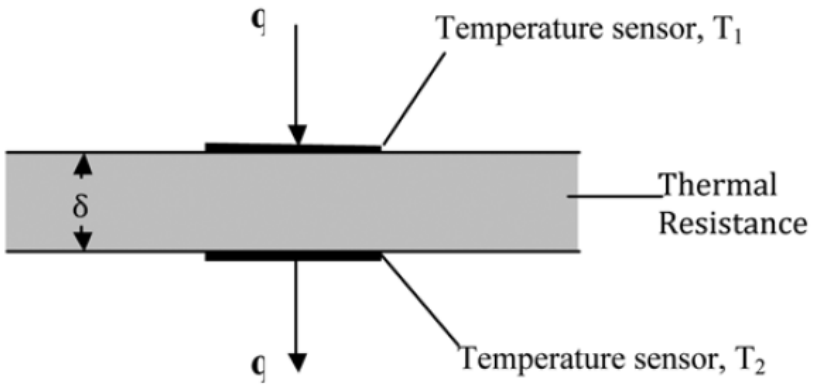

Figure 1.1. Diagram of one-dimensional heat flux through a thermal resistance layer of thickness δ [2]. Standard test method for measuring heat flux using surface-mounted one-dimensional flat gages, DOI: 10.1520/E2684-09, ASTM International, West Conshohocken, PA, 2009, www.astm.org (ASTM Standard E2684, 2009). Used under fair use, 2015.

where k is the thermal conductivity of the TRL, δ is the TRL thickness, T_1 and T_2 are the temperature of the top and bottom surfaces of the TRL, respectively. Depending on the direction of heat, the top or bottom surface will be at a higher temperature than the other. Differential temperature based sensors use either thermocouples, resistance temperature detectors (RTDs), or a combination of the two to measure surface temperatures. With these temperature measurements, in addition to knowledge of the thermal resistance layer (TRL) properties, the heat flux can be determined.

2.3.2. Resistance Temperature Detector Based Sensors

RTD heat flux sensors utilize resistance temperature detector methods to determine the temperatures of each surface of a TRL. RTDs use a small excitation current to measure the resistance of the known material which is a function of temperature. The RTDs directly measure the absolute temperature of each substrate surface then calculates the difference between them. This difference is usually a small fraction of a degree centigrade in thin-film sensors.

In general, the RTD method of measuring temperature is more accurate than thermocouple based temperature measurement but sensors using this method encounter a few difficulties. Most notably the materials electrical resistance used as the RTD are highly sensitive to strain changes caused by elongation/compression of the sensor and also material degradation due to aging. Thus RTD based sensors must be frequently calibrated in-situ in order for accurate measurements to be taken. For these reasons, RTD based sensors are not currently offered commercially and will not be discussed in detail in this paper.

2.3.3. Thermopile Gages

Thermopile gage sensors utilize the Seebeck effect to determine the temperature difference across a TRL. The Seebeck effect is a phenomenon that occurs when a homogeneous electrically conductive material experiences a temperature gradient across a spatial difference. An induced voltage is seen through the material that is proportional to the total temperature difference between the measurement locations. A measure of the strength of this induced voltage per degree Centigrade is a material intrinsic property called thermoelectric power, or Seebeck coefficient

$$Se = \frac{\Delta V}{\Delta T} \tag{1.2}$$

where ΔV is the induced voltage difference and ΔT is the experienced temperature difference. Thermocouples use this principle by connecting two electrically conductive materials together to form a measurement junction point. The thermocouple outputs a voltage

$$\Delta V = (Se_1 - Se_2) * \Delta T \tag{1.3}$$

where Se_1 and Se_2 are the absolute Seebeck coefficients of each individual thermocouple material. ΔT is the temperature difference between the temperature measurement junction point and the location of voltage measurement. For absolute temperature measurement using a thermocouple, an additional temperature measurement junction is required to be placed at a known temperature.

It is possible to use individual thermocouples to measure the top and bottom absolute temperatures of the TRL. Heat flux measurements utilizing this method are often extremely difficult to perform practically in a thin-film HFS due to relatively small temperature differences across the TRL, error in the thermocouples, and error in the known TRL properties. The thickness of the sensor, δ, and thermal conductivity, k, are not known with sufficient accuracy for any particular sensor to preclude direct calibrations of each sensor [3].

Thermopile based sensors mediate these issues by connecting the multiple thermocouples located on the top and bottom of the TRL in series. The individual thermocouple materials experience a temperature gradient as it connects from the top to the bottom surface of the TRL following equation 1.1. Unlike using an individual thermocouple where the voltage output is related to absolute temperature, the thermocouple materials in thermopile sensors are connected in series as junction pairs from the top to bottom TRL surface. Pairing the thermocouples in this manner results in a voltage output that is directly related to the temperature difference across the

TRL according to the absolute difference in the two Seebeck coefficients of the thermopile materials as in equation 1.3.

The output of a single thermocouple pair is often difficult to measure. The resulting voltage measurement is difficult because the effective temperature gradients across thin-film sensors are relatively small, usually a fraction of a degree Centigrade, and metals commonly used as thermocouple materials have Seebeck coefficients that are on the magnitude of 10 μV/C°. Thus output voltage signals could be lower than a single microvolt. A heat flux array (HFA) constructed by Ewing et al. [4] used single thermocouple pairs but required additional signal amplification equipment for taking measurements. A solution to small output signals is to connect multiple thermocouple pairs in series to amplify the induced voltage. The voltage differential output is amplified proportional to the number of thermocouple pairs, *N*

$$\Delta V = \frac{N\ Se\ q"\ \delta}{k} \tag{1.4}$$

where *Se* is the Seebeck coefficient of the combined thermocouple materials, *q"* is the heat flux conducted through the sensor, δ and *k* are the thickness and thermal conductivity of the TRL respectively. The majority of commercially available heat flux sensors (HFS) utilize this model in their sensor design.

2.4. Design Parameters of Heat Flux Sensors

Heat flux sensor performance can be characterized by a few parameters such as heat flux sensitivity, thermal resistance, sensor thickness, and response time. This section discusses each of these parameters and the desired characteristics in a heat flux sensor.

2.4.1. Sensitivity

The sensor sensitivity is the output voltage induced by the sensor divided by the heat flux conducted through the sensor

$$Sensitivity = \frac{\Delta V}{q''_{absorbed}} = \frac{N*Se*\delta}{k} \tag{1.5}$$

where N is the number of thermocouple pairs, Se is the Seebeck coefficient of the combined thermocouple materials, δ and k are the thickness and thermal conductivity of the TRL respectively. For ease of measurement, it is usually desired that a sensor have the highest sensitivity possible. Depending on the heat flux range being measured the sensitivity should be adjusted to ensure the voltage output is within the measurement device's detectable range.

2.4.2. Response Time

Response time is described as the time necessary for the sensor to report a change in heat flux from a step input change in absorbed heat flux. The parameter is based on the time in which it takes for the induced thermal energy to disperse and create a linear temperature gradient across the sensor TRL. The response time should be minimized so that the frequency response of the entire system is as quick as possible. Hager [5] gave the time required for 98% response in one-dimensional heat flux to be as follows

$$t = \frac{1.5\delta^2 \rho c_p}{k} \tag{1.6}$$

where t is time in seconds, δ is the thickness, k is the thermal conductivity, c_p is the thermal heat capacity, and ρ is the density of the TRL. It is common for companies to provide the time in which their sensor responds to 63% ($1\text{-}e^{-1}$) of the full output as the response specification for a HFS. This 63% or one time constant time response value is used in this paper.

2.4.3. Thickness and Thermal Resistance

Minimizing overall sensor thickness of a thin-film heat flux sensor is desired for a variety of reasons. With any thin-film heat flux sensor, using the sensor will inherently change the behavior of the heat transfer within the system. Placing it on a surface will add an amount of thermal resistance that would not exist in natural conditions. The thermal resistance of thin-film sensors is defined in equation 1.7.

$$R'' = \frac{\delta}{k} \tag{1.7}$$

Thus, minimizing the thickness, δ, or maximizing the thermal conductivity, k, will result in a sensor with the least amount of thermal resistance or thermal disruption to the natural heat flux. Decreasing the TRL thickness will also decrease the response time as defined by equation 1.6. Since this also decreases the sensitivity of the sensor, an optimization of the sensor for particular applications is usually necessary.

In scenarios where measuring forced convection heat transfer, placing the sensor on the measurement surface creates a protrusion that could potentially trip the boundary layer of fluid moving along the surface. Tripping a laminar boundary layer into turbulence would result in the fluid transferring a significantly larger amount of heat from the surface than it would under natural untripped laminar conditions. Therefore, a thin HFS is necessary in making accurate measurements.

2.4.4. Additional Heat Flux Sensor Design Considerations

In general, it is desired by the heat flux sensor user to have an inexpensive HFS with a high sensitivity, short time response, small thickness and very low thermal resistance. The

design of a HFS requires a significant amount of consideration to create a sensor with appropriate performance characteristics for the desired application.

Holmberg and Diller [6], determined that the only necessary requirements for correct operation of a HFS are that the bottom temperature sensors be at a uniform temperature and that the top temperature sensors are at a temperature determined by the amount of heat flux through the TRL. Using an encapsulation material with a high thermal conductivity is a method of creating a uniform temperature across the bottom temperature sensors. If a spatial temperature gradient exists on the measurement surface, a thermally conductive material on the outside of the sensor will distribute the heat and create a uniform temperature across the bottom surface temperature sensors.

2.5. Commercially Available Thermopile Heat Flux Sensors

The following section describes the construction design, performance characteristics and possible manufacturing techniques for various thermopile heat flux sensors that have been offered commercially. The performance specifications for each of these sensors are then compiled in Table 1.1 for ease of comparison between the different models.

2.5.1. RDF Corporation Micro-Foil (Version #1)

Orlando and Hines [7] first constructed Micro-Foil heat flux gages by manually wrapping combinations of either alumel and chromel or copper and constantan metallic foils as thermocouple materials around a polyimide Kapton thermal resistance layer substrate. The different metallic thermocouple material foils are individually butt welded together on either surface of the substrate to form the thermocouple junctions [3].

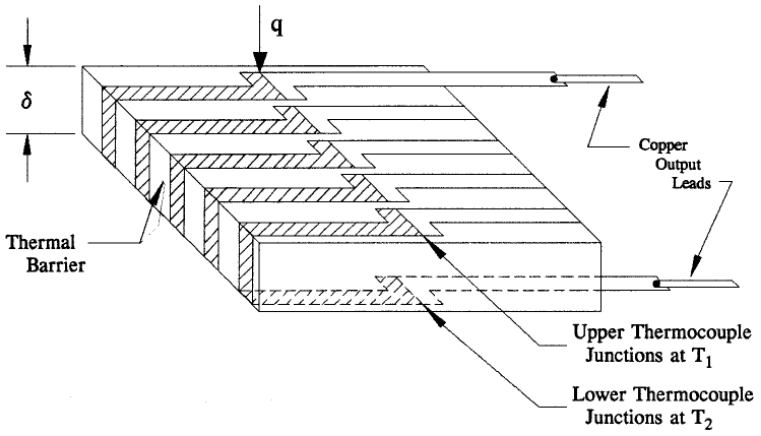

Figure 1.2. Diagram of the original Micro-Foil heat flux sensor designed by Orlando and Hines and sold by RDF Corporation. The sensor shown uses a copper/constantan thermopile that is wrapped around a thermal resistance layer and individually butt welded to form the thermocouple junctions [7]. D. J. Ortolano and F. F. Hines, A simplified approach to heat flow measurement. *Advances in Instrumentation*, Vol. 38, Part II, Research Triangle Park: ISA, 1983, 1449-1456. Used under fair use, 2015.

The Micro-Foil (Version #1) represents a valid sensor design because the thermocouple junctions are located nearly in line with one another across the TRL. The process of manufacturing the sensors themselves is difficult and intensive since each junction needs to be wrapped and welded together. These sensor models range in thickness and resulting sensitivities.

2.5.2. Vatell Episensor

Terrell [8] designed a thermopile sensor that was manufactured by Vatell Corporation through a process in which a photosensitive dielectric is patterned on an anodized aluminum substrate. The pattern is deposited so that there are troughs that will capture metallic paste as it is spread across the surface to create conductive paths once the paste is thermally cured. The photosensitive dielectric patterning and subsequent curing of two different conductive pastes is repeated twice in order to build a thermal resistance layer, electrical vias and thermocouple

junctions. Due to a large number of connected thermocouples (approximately 10,000 pairs), sensitivities are sufficient to measure heat fluxes as low as 0.1 (W/m^2) [3]. It is limited because the dielectric material is not very flexible and restricted to an operating temperature of 150 °C which is relatively low for a HFS.

2.5.3. BF Heat Flux Transducer

Vatell Corporation used nickel and copper plating processes to create a thermopile based HFS called the BF heat flux transducer [9]. The copper and nickel thermopile materials were plated through vias in the substrate to provide electrical connection from the top to bottom surfaces of the TRL.

2.5.4. Wire Wound Gages

The theory behind construction of a Schmidt-Boelter gage and similarly built heat flux sensors is described by Hauser [10]. The process begins with a thermal resistance layer that is wrapped in constantan wire. Half of the constantan wire material is then electroplated with copper while the other half of the constantan wire remains unplated. The constantan material remains continuous through the entire circuit but the copper is still effective in contributing to the thermocouple pair voltages. The copper has a significantly lower electrical resistivity compared to that of the constantan thus the copper plating creates an electrical short when placed in parallel with the inner constantan wire. The effective thermopile junctions are located where the copper plating ceases to exist at each point along the circuit path. Figure 1.3 below shows the basic construction of wire wound gages.

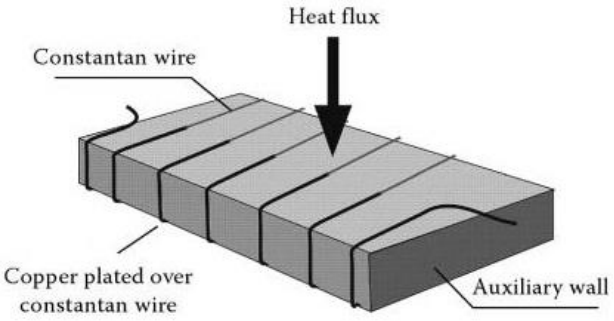

Figure 1.3. Diagram of a wire wrapped heat flux sensor. The thermal resistance layer is first wrapped with a constantan wire then half of the wire is copper electroplated to form the thermopile [11]. Orlande, Helcio R. B. *Thermal Measurements and Inverse Techniques*. Boca Raton, FL: CRC, 2011. Print. Used under fair use, 2015.

The Seebeck coefficient of the copper plated constantan combination is proportional to the ratio of Seebeck coefficient and electrical resistivity of each individual material. This manufacturing technique is not very adequate for the construction of thin-film heat flux sensors. The size of the overall sensor is limited by the precision of the wire winding and plating process. The electrical resistivity and resulting sensitivity must be uniform throughout the sensing area for precision measurements [12].

2.5.5. Heat Flux Microsensor (HFM)

Hager et al. [13,14] designed a sensor called the heat flux microsensor (HFM) which was later manufactured by Vatell Corporation through a high-vacuum sputtering process. The thermocouple materials of nickel and copper were patterned on an electrically insulating substrate in order to create the thermopile traces for the bottom surface. Silicon monoxide is then vapor deposited over the thermocouple traces in order to provide the TRL. Two more sputtering steps, one for each material is then conducted to pattern the top surface thermocouple junctions and also connect to exposed portions of the bottom traces to complete the thermopile.

Lastly, a silicon monoxide layer is again vapor deposited across the entire thermopile to electrically insulate and protect the thermopile.

The entire manufacturing process is very difficult and consuming. Each of the four sputtering processes require the precise alignment of a stainless steel mask and placed in a high-vacuum chamber before being conducted. The thermopile arrangement is seen below in Figure 1.4.

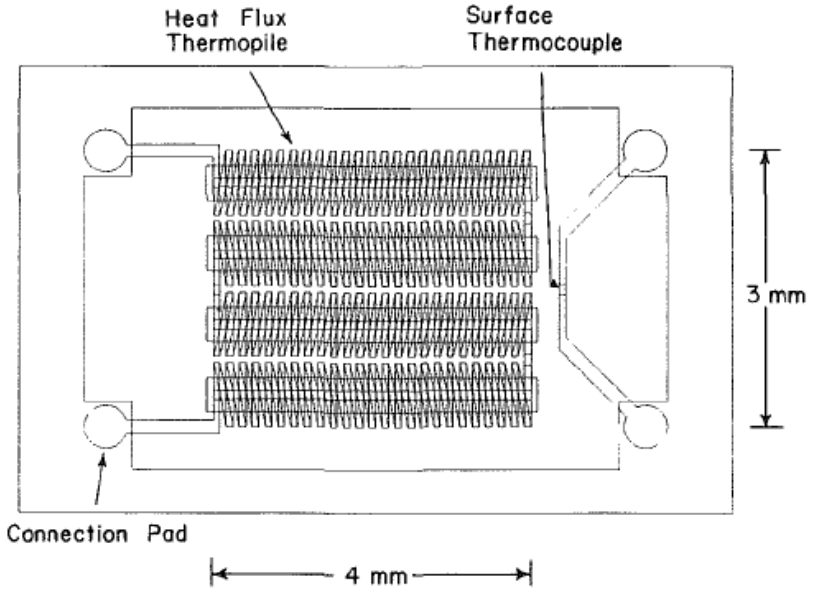

Figure 1.4. Heat flux microsensor gage pattern overlay [13]. Hager JM, Simmons SS, Smith DD, Onishi SS, Langley LW, Diller TE, Experimental Performance of a Heat Flux Microsensor. ASME. J. *Eng. Gas Turbines Power*. 1991;113(2):246-250. DOI: 10.1115/1.2906555. Used under fair use, 2015.

Sputtering provides an extremely thin thermopile of about 2 microns thick. This thin profile resulted in a small sensor thermal resistance and a very quick response time of 10 μs.

According to the one-dimensional heat flux assumption to Fourier's law made in equation 1.1, the thermocouple junction locations should be directly above one another on the thermal resistance layer substrate. Placing multiple thermocouple pairs in series to amplify the voltage signal as well as limitations in manufacturing capabilities often makes this arrangement difficult.

As mentioned previously, Holmberg and Diller [6] determined two thermal requirements for accurate operation of a HFS that made this arrangement not entirely necessary. Based on the two requirements of uniform bottom surface thermocouple junctions and top temperatures based on amount of heat flux, a second iteration of the thermopile gage was designed as seen in Figure 1.5.

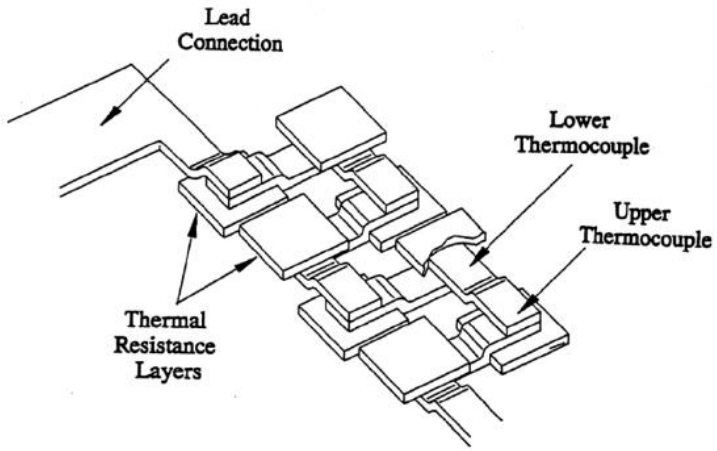

Figure 1.5. Diagram of thermocouple junction pairs layout in the second iteration of the heat flux microsensor [14]. J. M. Hager, S. Onishi, L. W. Langley, and T. E. Diller, High temperature heat flux measurements, AIAA J. *Thermophysics Heat Transfer*, 7, 531-534, 1993. Used under fair use, 2015.

The uniform lower temperature was achieved by using a high thermal conductivity substrate of aluminum nitride. The thermal resistance layer is provided by vapor depositing a layer of 18.1 μm thick silicon monoxide in locations where the upper thermocouple materials are then sputtered to form junctions. Initial designs then sputtered the thermal resistance layer on top of the bottom thermocouple junctions. For ease of manufacture, subsequent design iterations of the sensor did not include the final thermal resistance layer addition above the lower thermocouple junction. Due to the high thermal conductivity and small thickness of the TRL, the uniform heat flux is still achieved.

2.5.6. RDF Corporation Micro-Foil (Version #2)

The second version of the Micro-Foil heat flux sensor, currently produced by RDF Corporation, utilizes a similar thermopile layout to that of the HFM, assumedly for ease of manufacture. It appears that the thermocouple materials of copper and constantan are plated onto a polyimide substrate with the upper thermocouples located adjacent on an additional polyimide layer that provides the TRL as seen in Figure 1.6. The sensor is then coated with a conformal dielectric layer.

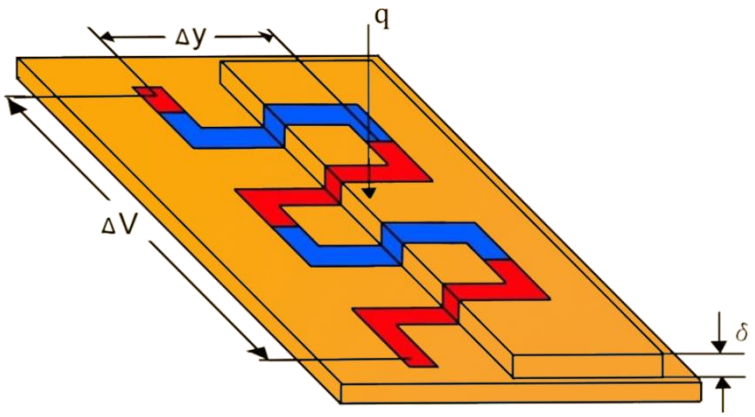

Figure 1.6. A partial layout schematic of the RDF Micro-Foil heat flux sensor version #2. The sensor uses a differential thermopile design using an offset thermal resistance layer of thickness δ. ΔV is the output voltage of the 2 thermocouple pairs depicted. Δy is the spatial difference in temperature measurement locations.

Although the RDF Micro-Foil Version #2 sensor is one of the cheapest sensors that is currently commercially available, there are underlying issues with the design layout that make accurate heat flux measurements difficult for certain heat transfer scenarios. Unlike the HFM, the second iteration of the Micro-Foil sensor does not use a highly thermally conductive substrate to ensure a uniform temperature across the lower thermocouple junctions. The polyimide substrate has a relatively low thermal conductivity that will cause heat to disperse slowly across the sensor causing uneven temperature distribution. Also, a polyimide TRL is not placed on top of the lower thermocouple junctions so there is uneven thermal resistance across the sensor. This means

that the thermal resistance layer beneath the upper thermocouple junctions is in parallel with no TRL seen by the lower thermocouple junctions. Since the thermal conductivity of the TRL is relatively low, more heat will transfer through the lower junctions than the upper junctions and thus create error in measurements. Lastly, the conformal dielectric coating also creates a non-uniform sensor surface that creates uneven thermal contact resistance if not applied correctly which also contributes to non-uniform heat flux through the sensor.

2.5.7. Specifications of Commercially Available Heat Flux Sensors

The specifications of sensitivity, response time, sensor thickness and quoted retail cost for a variety of heat flux sensors and compiled in Table 1.1. Some specifications such as sensitivity and cost range depending on the specific model of the heat flux sensor that utilizes the general construction technique and layout design.

Table 1.1. Compiled performance specifications of various heat flux sensors that have been commercially available.

Heat Flux Sensor	Sensitivity ($mV/(W/cm^2)$)	Response Time (s)	Thickness (microns)	Currently Available? (Yes/No)	Cost ($)
Micro-Foil (Version #1)	0.63 – 34.7	0.02 – 0.4	76 - 330	Yes	500 - 835
Episensor	8.35	1.0	350	No	250
BF Heat Flux Transducer	0.5 – 10	0.9	200	No	150
Schmidt-Boelter	0.150	0.5	N/A	Yes	500 – 1,300
Heat Flux Microsensor	0.150	$17x10^{-6}$	22	Yes	2,880
Micro-Foil (Version #2)	8.201	0.13	165	Yes	210 - 615

It should be noted that the thickness of the Schmidt-Boelter gage is not listed since it is not a thin-film heat flux sensor like the other sensors described in this paper.

2.6. Experimental Construction of PHFS

This section describes the rationale used in determining the PHFS design as well as the manufacturing process used to produce the final sensor product. A more detailed, step-by-step description of the manufacturing process can be found in Appendix A.

2.6.1. PHFS Design Decisions

The overall goal of designing the PHFS was to decrease the manufacturing cost of the sensor while maintaining sensor performance of the final product. Multiple methods of manufacturing heat flux sensors, such as inkjet and extrusion printing, electroless plating and electroplating, and flexography, were investigated to determine feasibility in achieving these goals. Multiple issues arose with each of these processes but the general problems were that the processes are labor intensive and/or did not use the materials necessary to create a thermopile. After performing concept selection on the manufacturing process choices, a combination of copper etching and stencil printing conductive inks was chosen. A flowchart of the overall process that was designed is shown in Figure 1.7.

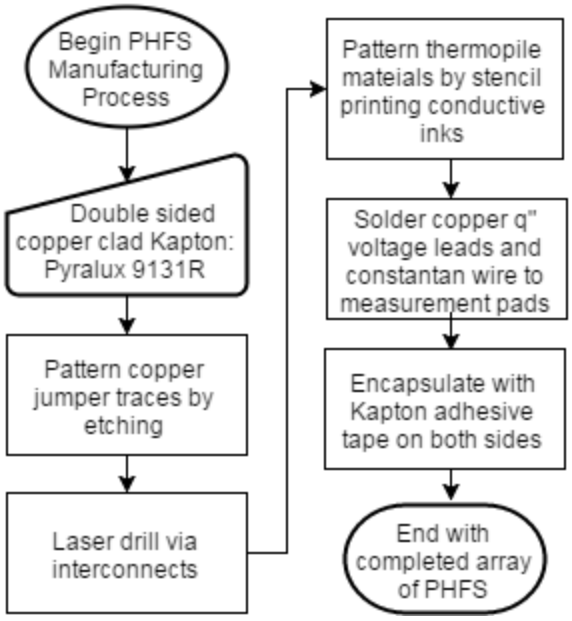

Figure 1.7. Flowchart of the manufacturing process used to produce the PHFS. It combines copper etching for jumper connections and stencil printing metallic nickel/silver ink thermopile materials.

During the design process and initial testing, decisions were made about the construction of the PHFS that gave it similar attributes to previously manufactured sensors. The PHFS is like the Vatell Episensor because it uses printed metallic conductive ink as the thermopile materials. Unlike the Episensor which uses a photosensitive polymer substrate, the PHFS uses a flexible Kapton substrate that allows a thinner sensor profile, higher operating temperature, and greater sensor flexibility. The PHFS has laser-drilled electrical vias similar to that of the BF heat flux transducer. This facilitates electrical connection from the top to bottom layer of the TRL without wrapping the connections around the TRL as seen in alternative HFS designs. A basic schematic of how the PHFS is constructed for two out of the 72 thermocouple junction pairs is shown in Figure 1.8

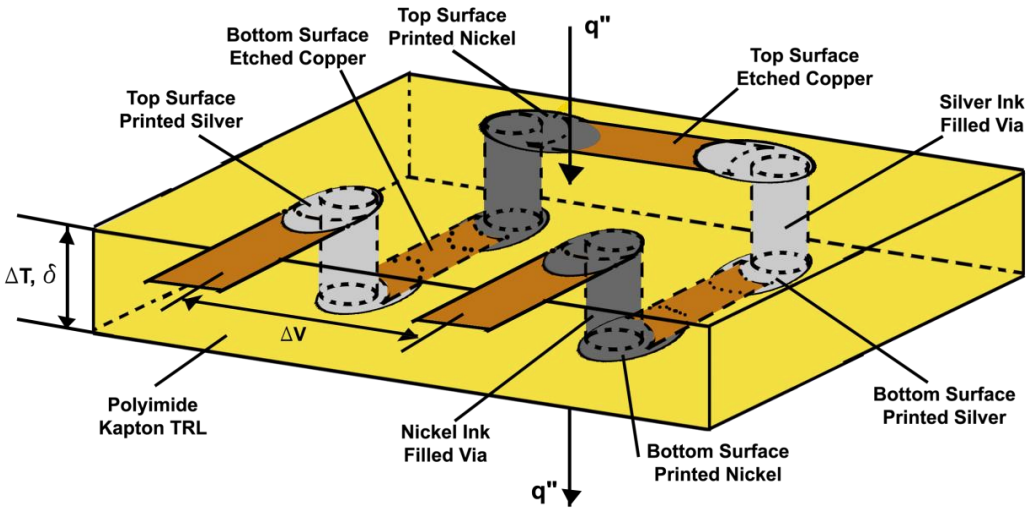

Figure 1.8. Schematic of the PHFS construction layout for two thermocouple junction pairs. The nickel and silver ink printed through the vias act as the thermopile materials. The etched copper traces are jumper connections between each via.

where ΔV is the output voltage from the two thermocouple junctions pairs. The output voltage is induced as the nickel and silver ink thermopile materials filled in the vias connect across the polyimide Kapton TRL of thickness, δ, and experience the temperature differential, ΔT, created by the absorbed heat flux, q''.

Using this construction technique it is possible to produce a sensor that is flexible, similar thickness, thermal resistance and response time to other heat flux sensors. Due to limitations in the precision of stencil printing, the ratio of sensitivity to overall sensing area of the PHFS may be lower than currently manufactured sensors.

2.6.2. Copper Etching

The manufacturing process used to produce the printed heat flux sensor described in this paper begins with a double sided copper cladded polyimide Kapton manufactured by DuPont, Pyralux AP 9131R. Pyralux AP 9131R consists of a 76 micron thick polyimide Kapton with a 1 oz. weight or 35 micron thickness of copper clad on either side. Using copper etching, the double

sided copper is patterned into circuit traces shown in Figure 1.9 along with the laser drilled vias performed in the next manufacturing step.

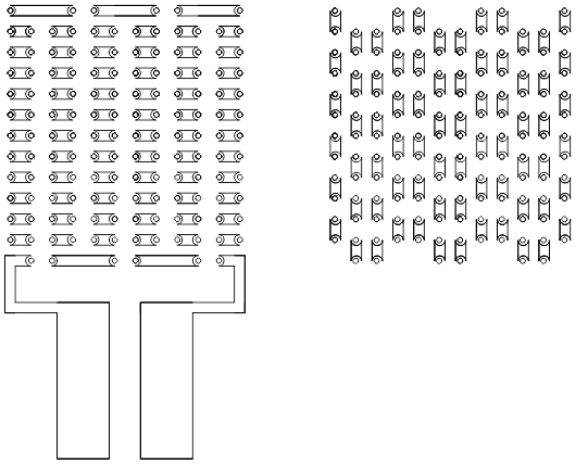

a) **b)**

Figure 1.9. Picture of the copper trace designs and laser drilled via holes for both the **a)** top and **b)** bottom surfaces of the PHFS.

A more detailed, dimensioned diagram of the copper etched design is shown in Appendix A. In order to pattern and perform the etching a photosensitive dry film resist is laminated to both copper surfaces of the AP Pyralux using a hot roll laminator. Reusable opaque acrylic stencil masks are laser cut using a V-460 laser cutting system according to the dimensions in Apendix A. The opaque acrylic stencil mask jig is used to enclose the sensitized AP Pyralux as it is exposed to 12 minutes of light provided from a 250W halogen lamp. The cut patterns are the areas that will be the areas of copper traces located on the PHFS circuit.

2.6.3. Laser Drilling Vias

During the next step, vias with diameters of 180 microns are then laser drilled through the PHFS polyimide Kapton substrate using the V-460 laser cutting system. These vias are used to provide interconnects for the thermopile materials to be placed through to electrically connect from the top to bottom surfaces of the TRL. During preliminary testing, the vias were

mechanically drilled with a similar diameter but issues arose with the conductive ink connections through these holes. The reasoning behind these unstable via connections was assumed to be caused by the edge burring that occurred due to the mechanical drill bit which caused uneven surfaces for the ink to print through.

2.6.4. Stencil Printing Thermopile Materials

The V-460 laser cutting system is used to cut four individual reusable printing stencils corresponding to each of the printed ink designs into separate pieces of 76 micron thick polyimide Kapton. The four stencils are seen in Appendix A and used for printing each of the following designs: silver ink on the top surface, nickel ink on the top surface, silver ink on the bottom surface, and nickel ink on the bottom surface. The stencil printing process of the thermopile materials follows the following procedure using their appropriate printing stencils.

1. The first thermocouple material, EMS C-1001 silver ink, is stencil printed onto the top of the TRL surface through half of the electrical vias and thermally cured in a box oven at 130 °C for 10 minutes.
2. The second thermocouple material, EMS C-5001 nickel ink, is stencil printed onto the top of the TRL surface and also through the remaining vias. The nickel ink is then thermally cured in a box oven at 130 °C for 10 minutes.
3. Printing the silver and nickel conductive ink from steps 1 and 2 is repeated on the bottom surface of the sensor to ensure stable electrical connections to complete the heat flux sensor circuit.

The ink makes electrical connection to the copper traces on either surface of the polyimide Kapton. Each of the materials also transverse the two layers of the TRL to make thermocouple junction pairs.

2.6.5. Detailed Design of PHFS

The PHFS design utilizes a differential thermopile arrangement that measures the temperature difference across a 76 micron thick dielectric Kapton substrate TRL. The thermocouple materials consist of EMS silver C-1001 and EMS nickel C-5001 conductive inks that are patterned onto the sensor using stencil printing. The size of the via holes cut by the laser cutter is set to a diameter of 180 microns to facilate the largest volume of ink which coats the inside barrel of the via to provide stable electical connections while also minimizing copper space widths.

The copper trace widths are 740 microns while the trace spacings are 1240 microns to allow some error in printing bleed beneath the stencils. Thickness of the deposited ink is approximately equal to the thickness of the 76 micron thick stencil used during printing. The copper trace pattern zig-zags side to side so that the thermocouple pairs are as close as possible to one another to minimize error caused by one-dimensional heat flux assumption. The total sensing area of the PHFS has a width of 23 mm and length of 25 mm.

Measurement pads, consisting of copper traces, extend nearly 18 mm outside the sensing area to provide soldering points for copper wires used for heat flux voltage measurements. An additional 250 diameter constantan wire (TFCC-010) supplied from Omega is soldered to one of the measurement pads to create a type-T thermocouple with one of the copper wires so that a

sensor surface temperature can be also measured. Thus, from a total of three wires, it is possible to determine heat flux absorbed by the sensor as well as sensor surface temperature.

The voltage leads are made of the same 250 micron diameter thermocouple grade copper wire (TFCP-010) supplied by Omega and are connected to the measurement pads located close to one another so that it can be assumed the lead connections are at the same temperature. This ensures the voltage leads experience the same temperature gradient from the measurement pads to the voltage measurement location so the influence of their thermoelectric voltages is negated. The copper traces within the sensing area circuit are used to provide stable electrical jumper connections from one via to the next. The copper does not act as a thermocouple material since it does not move across the TRL and therefore does not experience the temperature gradient from T_1 to T_2 described in equation 1.1. Figure 1.10 shows the PHFS after both the CI-1001 silver and CI-5001 inks are printed and the three wire leads are connected.

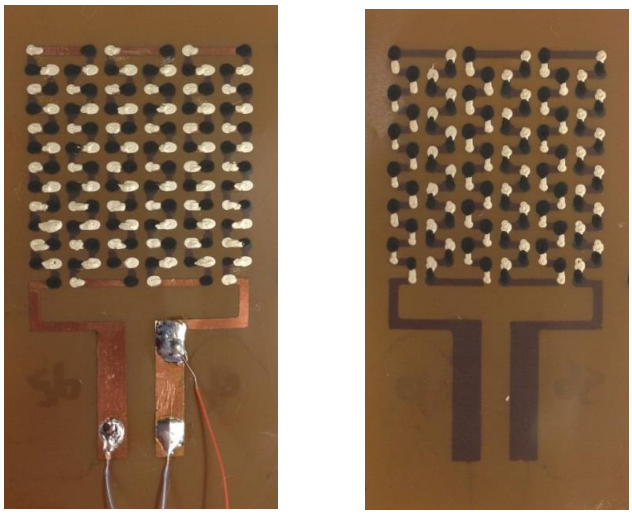

a) **b)**

Figure 1.10. Picture of the PHFS **a)** top and **b)** bottom surfaces. The black material is CI-5001 nickel ink while the silver material is CI-1001 silver ink printed on 76 micron thick Kapton substrate. Two blue copper leads are soldered to the base of the measurement pads for heat flux voltage measurement. A red constantan wire is soldered to one measurement pad to provide a type-T thermocouple temperature measurement when used in conjuction with one of the copper leads.

For ease of manufacturing a buffer area exists surrounding each sensor where no circuit traces exist. This buffer area increases the total sensor size from 42.4 x 23.1 mm to 55.1 x 35.8 mm or 19.7 cm^2. The last step in manufacturing the PHFS is to electrically encapsulate the sensor by placing a 25.4 micron thick Kapton film tape with 38.1 micron thick silicon adhesive on both the top and bottom surfaces. A detailed step by step description of the manufacturing process is shown in Appendix A.

2.7. Experimental Equipment and Methods

This section describes the various experimental facilities and equipment used to manufacture and test the printed heat flux sensors (PHFS) produced by using the novel manufacturing process. It also describes the experimental methods designed for these systems to characterize PHFS performance by determining the Seebeck coefficient of the combined CI-1001 silver/CI-5001 nickel ink thermocouple, PHFS sensitivities through radiation and conduction calibrations, and time response of the PHFS.

2.7.1. Instrumentation

Data acquisition for this paper was performed using a 9214 National Instruments DAQ unit in conjunction with Labview software. The 9214 DAQ has a 24-bit resolution for its Delta-Sigma analog to digital converter with a maximum sample rate of 100 Hz. The 9214 DAQ is for thermocouple temperature and voltage measurements. It was used during radiation calibrations, conduction calibrations and Seebeck coefficient testing. Data for these tests was sampled at a rate of 1 Hz.

The 9214 DAQ was also used to perform data acquisition for measuring the time response of the PHFS. A PHFS output voltage measurement sample rate of 75 Hz was used during time response data runs. This higher sampling rate is more appropriate for measuring the transient voltage signals seen during PHFS time response.

2.7.2. Laser Cutting System

The V-460 laser engraving and cutting system located in the ROMELA lab at Virginia Tech was used for aiding in various manufacturing steps to produce the PHFS. The V-460 was used to cut acrylic masks used for copper etching, laser drill via holes through the PHFS substrate, and cut printing stencils into Kapton for conductive ink patterning.

The V-460 laser (Universal Laser Systems) is a 50W CO_2 class III laser. It has a work bed area that measures 609 x 457 mm. Vector based designs can be created in CorelDraw graphics software. Before the laser is operated, laser power and laser head movement speed can be specified by the user depending on the material being cut or engraved.

2.7.3. Seebeck Coefficient Testing Setup

Heat flux sensor sensitivity depends on TRL thickness, TRL thermal conductivity, thermocouple Seebeck coefficients, and number of thermocouple junction pairs according to equation 1.5. Since the metallic conductive inks used as the thermocouple materials consist of components in addition to their respective bulk materials it was necessary to measure the Seebeck coefficients. The ink materials were printed to form a single thermocouple junction. The Seebeck coefficient, Se, of the combined ink materials is the measured voltage output, ΔV, from the thermocouple across a temperature differential, ΔT.

$$Se = \frac{\Delta V}{\Delta T} \tag{1.8}$$

The thermocouple junction is insulated and heated using a resistance heating unit that is connected to a DC voltage supply. The other end of the thermocouple is kept insulated at room temperature and connected to voltage measurement leads. Type T surface thermocouples are used to measure the temperature of the specimen at the heated junction point as well as the voltage measurement location. A diagram of the experimental setup used to measure the Seebeck coefficient is seen in Figure 1.11.

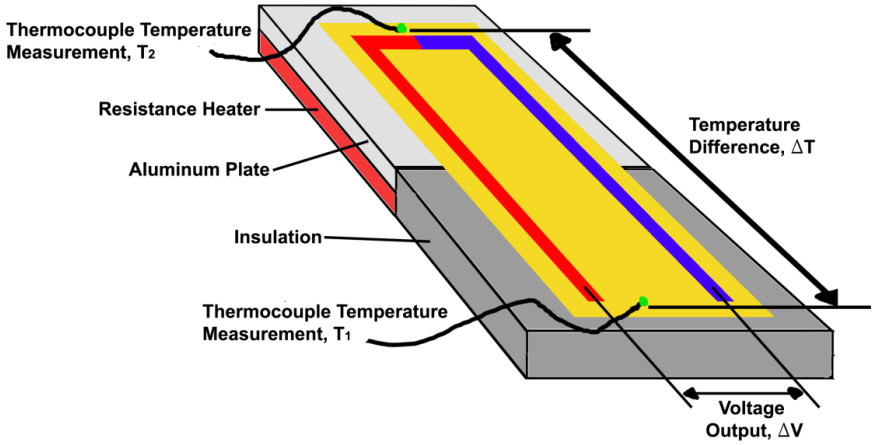

Figure 1.11. Diagram of the experimental setup used to measure the Seebeck coefficient of a single thermocouple junction. Printed conductive metallic nickel and silver inks shown as red and blue materials. Output voltage is measured as a function of induced temperature difference.

The voltage measurement locations are also insulated so that the leads remain at the same temperature as one another to ensure that they do not contribute to the thermoelectric voltage themselves.

2.7.4. Conduction Sensitivity Calibration Setup

Sensor calibration can be performed using conduction heat transfer through the use of the following experimental setup and procedure. A more detailed procedure can be found in

Appendix C. The printed heat flux sensor is placed directly on top of a reference RDF Micro-Foil heat flux sensor which has a known sensitivity of 1.870 uV/(W/m^2). The area surrounding both of the sensors is filled with a polyimide Kapton masking layer of the same thickness as the sensors. The stacked sensors are placed between silicone gap pad conformal layers, then between a water-cooled plate and a resistance heating element and pressed together using a large weight to minimize the thermal contact resistance between all of the components. The entire setup can be seen in Figure 1.12.

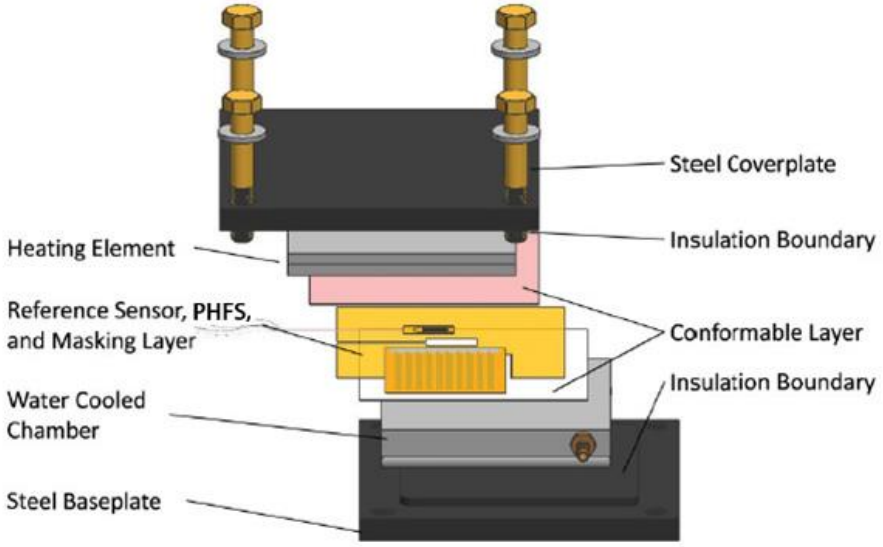

Figure 1.12. Diagram of a steady-state conduction sensitivity calibration facility. Heat flux is maintained between the upper heated plate and the bottom water-cooled plate [4]. Ewing, Jerrod, Andrew Gifford, David Hubble, Pavlos Vlachos, Alfred Wicks, and Thomas Diller. "A Direct-measurement Thin-film Heat Flux Sensor Array." *Measurement Science and Technology Meas. Sci. Technol*.21.10 (2010): 105201. *Iopscience*. Web. 8 Aug. 2015. Used under fair use, 2015.

Heat flux is induced through the sensors by varying the temperature of the heating element and/or the water coolant. Since the heat flux is one-dimensional and the sensors are located directly on top of one another it can be assumed that each sensor is experiencing the same heat flux.

During each data run the sensors were tested through a range of approximately 0 to 2500 W/m^2 induced heat flux. The voltage outputs of both the reference RDF heat flux sensor and the PHFS are measured simultaneously using a 24-bit DAQ system sampling at 1 Hz and recorded using Labview. Sensitivity of the test sensor is calculated using the voltage measurements as well at the reference sensor sensitivity according to equation 1.9 as follows

$$S_{PHFS} = \frac{V_{PHFS}}{q"_{absorbed}} = \frac{V_{PHFS} S_{ref}}{V_{ref}} \tag{1.9}$$

where V_{PHFS} is the output voltage of the printed heat flux sensor, $q"_{absorbed}$ is the absorbed heat flux through the sensor, S_{ref} is the sensitivity of the reference heat flux sensor, and V_{ref} is the voltage output of the reference heat flux sensor.

2.7.5. Radiation Sensitivity Calibration Setup

Sensor calibration can be performed by using radiation heat transfer through the use of a substitution radiation calibration system. The system uses an array of three 250 W halogen lamps connected to a variable AC voltage regulator as a radiation heat source. The enclosure surrounding the lamps, as well as the surface behind the mounting location of the sensor, is cooled using room temperature circulating water. The water cooling maintains the enclosure at a steady temperature as well as provides a heat sink for the radiative heat flux created by the lamps as it is absorbed and flows through the heat flux sensor being calibrated. Cooling water also maintains the sensor being calibrated at a constant temperature so that natural convection effects off the face of the sensor can be minimized.

The radiation calibration system is first calibrated using a Schmidt-Boelter reference gage with a known sensitivity value of 625 uV/(W/cm^2) . Absorbed heat flux measured into the gage from the lamps is plotted as a function of input voltage supplied to the halogen lamps. The PHFS

being calibrated is spray painted with Aervoe Z635 Black Zynolyte High Temp Paint with a known emissivity value of 0.94 before being mounted into the calibration system. The lamps are powered at a variety of input voltages between 40 and 120 V while being measured by a HP 3468A multimeter. The absorbed steady-state heat flux is calculated using a Matlab program that is found in Appendix E. Simultaneously the output voltage from the PHFS is measured by a NI 9214 24-bit DAQ system at a sampling rate of 1 Hz.

2.7.6. Time Response Experimental Design

The radiation calibration system was used to measure the time response of the PHFS. The system was set to output a steady-state level of radiative heat flux originating from an array of three halogen lamps. An opaque shutter is placed between the radiation heat source and the PHFS which is mounted to a water-cooled metal surface. The shutter is removed at a rate of approximately 20 m/s to simulate a step input of heat flux from zero to between 0.3 – 2.0 W/cm^2 absorbed into the PHFS. The PHFS output voltage response is measured by a 9214 NI-DAQ system at a rate of 75 Hz and recorded as a function of time until the sensor reaches the full value of output voltage corresponding to the steady state absorbed heat flux. The amount of time required for the sensor to report 63% (1-e^{-1}) of the final steady state output is taken as the response time.

2.8. Results and Discussion

The following section describes the results obtained during experimental testing of the PHFS. Seebeck coefficient of the conductive ink thermocouple, PHFS sensitivity and time response was determined.

2.8.1. Seebeck Coefficient Results

A total of five individual thermocouple junctions were printed and each was tested four times for a total of 20 data runs with about 41,000 data points of temperature difference and voltage measured by a 9214 DAQ with 24-bit resolution Delta-Sigma A/D converter at a rate of 1 Hz. Throughout each data run the temperature of the test thermocouple junction was varied using a resistance heater. The minimum and maximum experienced temperature differential between the junction point and the measurement location was 1.7 and 50.9 °C respectively. The data was collected in a LabVIEW program and analyzed using a Matlab code which can both be found in Appendix E. The data was compiled and a least squares regression was performed and plotted in Figure 1.13.

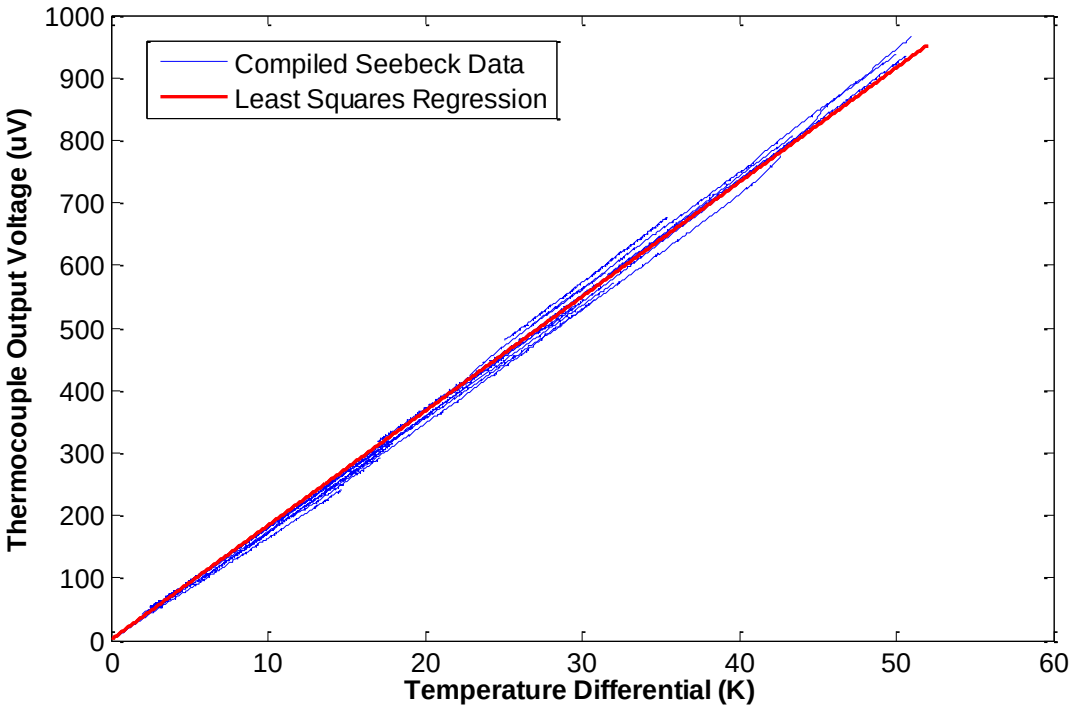

Figure 1.13. Plot of the least squares regression fit model used to determine Seebeck coefficient of the metallic conductive ink thermocouple. Least squares regression was performed on 41,000 compiled data points of output voltage and measured temperature difference. The slope of the line is equal to the Seebeck coefficient with a value of 18.3 ± 0.9 uV/°C.

The average Seebeck coefficient of the thermocouple junctions formed using EMS CI-1001 silver ink and CI-5001 nickel ink is 18.3 ± 0.9 uV/°C. This value deviates from the value for Sebeeck coefficient for bulk nickel and bulk silver of 21.5 uV/°C. This deviation from bulk material Seebeck values is expected since conductive inks are formulated from a mixture of their bulk material metallic particles, an epoxy adhesive, and a solvent thinner. Some inks consist of additional ingredients that facilitate alternative curing methods besides thermal curing which can also contribute to changes in their thermoelectric properties.

The expected PHFS sensitivity is calculated in equation 1.10 using the measured value of Seebeck coefficient, along with number of thermocouple junction pairs, Kapton TRL thickness of 76 microns and thermal conductivity of 0.12 W/(m-K) reported by DuPont [15].

$$Sensitivity = \frac{\Delta V}{q''_{absorbed}} = \frac{N*Se*\delta}{k} = \frac{(72)\left(18.3\pm0.9\frac{uV}{K}\right)\left(7.60x10^{-5}\ m\right)}{\left(0.120\left(\frac{W}{m-K}\right)\right)} = 0.834\frac{uV}{\left(\frac{W}{m^2}\right)} \quad (1.10)$$

Thus the expected sensitivity for the PHFS using these values is 0.834 uV/(W/m^2) or 8.34 mV/(W/cm^2).

2.8.2. Conduction Sensitivity Calibration Results

A sample of 12 PHFS were tested at least four times each for a total of over 57,000 measured voltage data points while using the conduction calibration system. The measured sensitivities of each PHFS are plotted in Figure 1.14.

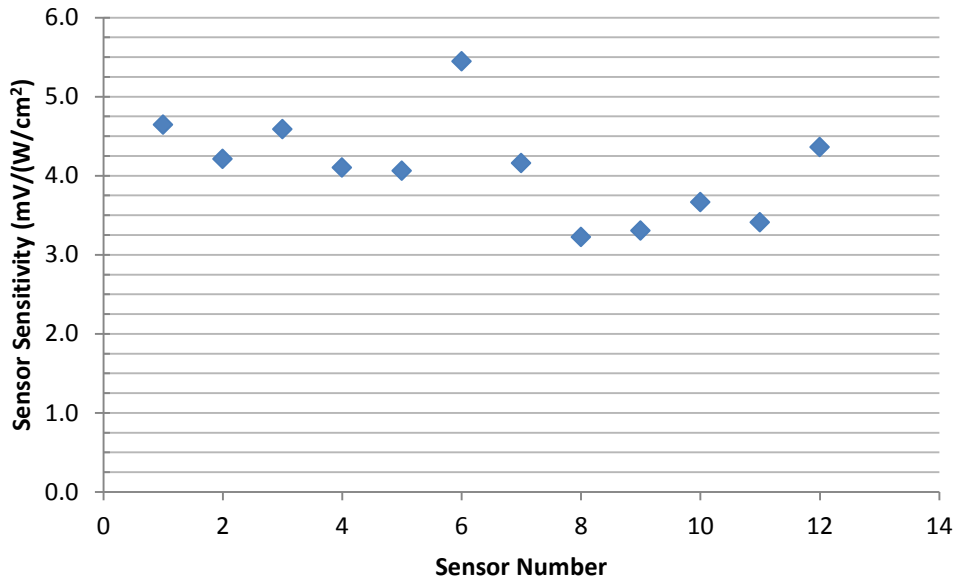

Figure 1.14. PHFS sensitivities measured using the conduction sensitivity calibration system. The data represents a sample of 12 sensors out of a total of 80 manufactured. The average sensitivity is 4.10 ± 0.23 mV/(W/cm^2) with a maximum of 5.45 mV/(W/cm^2), and minimum of 3.22 mV/(W/cm^2).

An average sensitivity value of 4.10 ± 0.23 mV/(W/cm^2) was measured out of the sample of 12 sensors. This average value is 51% smaller than the expected theoretical sensitivity value of 8.34 mV(W/cm^2) calculated using equation 1.10. It is suspected that this deviation from the expected theoretical sensitivity is caused by inaccuracy of the Kapton thermal conductivity value provided by DuPont. The ASTM standard test performed and cited by DuPont, ASTM F-433-77 (1987), is a method for determining thermal conductivity of gaskets and likely not appropriate for accurately evaluating the thermal conductivity of the thin-film Kapton material.

A more adequate method of measuring the thermal conductivity of Kapton was performed by Ewing et al. [4] using a calibrated heat flux array constructed with vapor deposited thermocouple junctions for direct surface temperature measurements. Using this method, Ewing reported a measured thermal conductivity value of 0.288 W (m K)$^{-1}$. Jacquot et al. [16] used sputtered thermocouple films, with minimal thermal contact resistance, to directly measure the

temperature difference across Kapton film. Using this method, a thermal conductivity value of 0.32 W (m K)$^{-1}$ was measured for the Kapton film.

Using the measured value for Seebeck coefficient of the nickel/silver ink thermopile materials, Se, along with the other known parameters of the PHFS, the thermal conductivity, k, is calculated to be 0.244 W (m K)$^{-1}$ in equation 1.11

$$k = \frac{N*Se*\delta}{S} = \frac{(72)\left(18.3\,\frac{uV}{K}\right)\left(7.60x10^{-5}\,m\right)}{\left(0.410\left(\frac{\mu V}{W/m^2}\right)\right)} = 0.244\,\frac{W}{m-K} \qquad (1.11)$$

where N is the number of thermocouple junction pairs, δ is thickness of the Kapton TRL substrate, and S is the measured PHFS sensitivity. This value is over twice the value of 0.12 W (m K)$^{-1}$ reported by DuPont and supports the claims made by Ewing et al. and Jacquot et al. that the DuPont value for thermal conductivity is inaccurate.

2.8.3. Radiation Sensitivity Calibration Results

A sample of three PHFS's were calibrated using the radiation calibration system four times each for a total of 12 data runs. A total of 4900 PHFS voltage data point measurements were recorded over a range of 0 to 2 W/cm^2 absorbed radiative heat flux. 120 PHFS output voltage samples are taken for each steady-state radiative heat flux event, then averaged together and plotted as a function of net absorbed heat flux as seen in Figure 1.15.

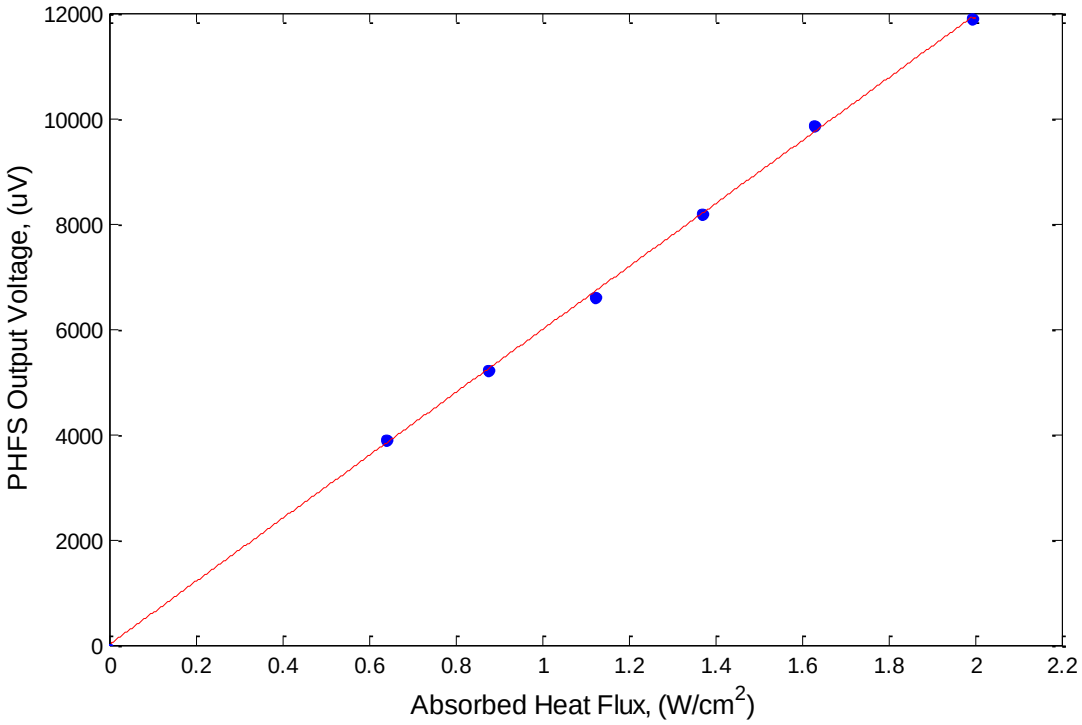

Figure 1.15. PHFS voltage output as a function of absorbed heat flux while mounted in the radiation calibration system. Averaged measurements during six steady state radiative heat flux events are shown by markers. The slope of the least squares regression line for these measurements is the sensor sensitivity with a value of 3.57 ($mV/(W/m^2)$) for this particular PHFS.

A least squares regression was performed to determine the average PHFS sensitivity for each data run. The average measured PHFS sensitivity for the sample of three different PHFS's tested using the radiation calibration system is 4.24 ± 0.13 $mV/(W/cm^2)$ with a maximum and minimum sensitivity of 4.92 and 3.57 $mV/(W/cm^2)$ respectively. The average measured sensitivity is 3.30% higher than that measured using the conduction calibration system. Sensitivity measurements taken using the radiation calibration system are within the uncertainty of those taken with the conduction calibration system. These results also support the claim of inaccuracy in the value of thermal conductivity reported by DuPont.

2.8.4. Time Response Results

A total of 42 data runs with 160,000 transient output voltage data points were measured at 75 Hz by a 9214 DAQ to determine the time response of the PHFS. The voltage output of a PHFS was normalized to an average full steady-state voltage output. The transient voltage response signal was plotted as a function of time. The time response of the PHFS for each data run was then averaged together and the resulting calculated average voltage output transient response is plotted as a function of time as seen in Figure 1.16.

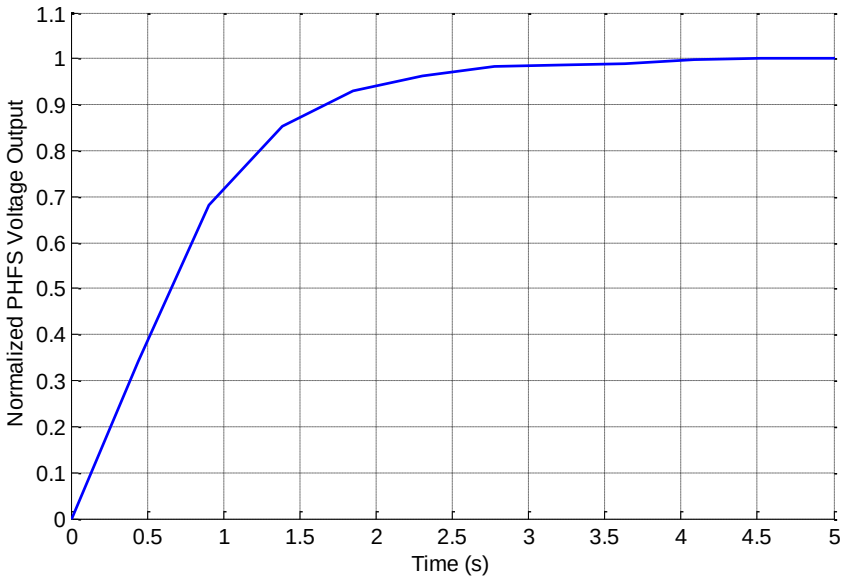

Figure 1.16. Normalized average PHFS heat flux output voltage as a function of time in response to a step input. The average response for 63% of the full value is 0.592 ± 0.026 seconds.

It was determined that the average response time of the PHFS is 0.592 ± 0.026 s for one time constant, or 63% of the full output voltage signal.

2.8.5. Cost Analysis Results

The driving motivation for conducting the research discussed in this paper is to reduce the overall cost of the final HFS product. Once the manufacturing process had been proven

effective in consistently producing functional sensors, a cost analysis was performed to estimate total material costs required.

The total sensor area size of 19.7 cm^2 is used in the cost analysis to determine the necessary amounts of Pyralux AP 9131 copper clad Kapton used as the substrate. The sensor size is also used to estimate the amount of dry photoresist film lamination and ferric chloride used for patterning and etching the copper trace design. Note that the required area of these two materials is doubled to 39.4 cm^2 since etching is required on both sides of the Pyralux AP 9131 substrate.

While manufacturing the PHFS, it was determined that an average of 0.3 grams of CI-5001 nickel ink and 0.2 grams of CI-1001 silver ink is deposited onto each sensor. The material unit costs, necessary amount of the material required in manufacturing the PHFS, and total material costs per sensor are listed in Table 1.2.

Table 1.2. Materials required for manufacturing the PHFS.

Manufacturing Material	**Unit Cost**	**Quantity per Sensor**	**Cost per Sensor**
EMS C-5001 Nickel Ink	\$0.54/gram	0.3 grams	\$0.16
EMS C-1001 Silver Ink	\$0.98/gram	0.2 grams	\$0.20
Pyralux AP 9131 Copper Clad Kapton Substrate	\$93.00/m^2	19.7 cm^2	\$0.18
Ferric Chloride Etching Solution	\$46.5/m^2	39.4 cm^2	\$0.18
Dry Photoresist Film Lamination	\$31.00/m^2	39.4 cm^2	\$0.12
25 mm Width Kapton Tape Encapsulation	\$0.26/m	55.1 mm	\$0.01
			Total Cost: \$0.85

The total estimated cost of materials necessary to manufacture the PHFS is \$0.85. This cost represents the price of materials used in just the sensor itself and does not include the cost of wire voltage leads.

Cost of labor is estimated by taking the average time required to complete each of the manufacturing steps. Table 1.3 depicts the average time for each step in the process to be

completed as well as the amount of time that a worker would spend dedicated to performing the specific manufacturing task. The time required to complete each of the manufacturing tasks listed in Table 1.3 were recorded while a single person worked to produce arrays of four sensors per manufacturing batch.

Table 1.3. Breakdown of manufacturing steps necessary to produce an array of four PHFS's.

Manufacturing Task	**Required Task Time (minutes)**	**Required Dedicated Labor Time (minutes)**
Dry Photoresist Film Laminated onto Substrate	5	5
Attach mask and expose to light source	20	10
Etch Copper Traces	60	10
Laser Drill Vias	6	5
Manually Stencil Print Conductive Inks	25	25
Cure Conductive Inks	40	1
Encapsulate in Kapton Tape	8	8
Sum	**164**	**64**

It was determined that approximately 164 minutes of total manufacturing time and 64 minutes of dedicated labor time are required on average to manufacture an array of four PHFS's. Therefore an average of 41 minutes of manufacturing time and 16 minutes of dedicated labor time are spent per PHFS. Assuming a rate of $20.00/hr for labor would result in a total labor cost of $5.33 per PHFS. Thus a total combined cost of material and labor per PHFS, if the sensors are manufactured in arrays of four per manufacturing batch, is $6.18.

Over the course of manually constructing 80 PHFS's, a manufacturing yield of 80% was seen. It was found that the 20% of defective sensors produced was caused by errors in the one or more printing conductive ink manufacturing step(s). Frequently the defective sensors could be

fixed by repeating one of the printing steps. Assuming an 80% yield and applying this to the manufacturing cost, a final manufacturing cost of $7.73 was calculated.

The sensors that were manufactured for testing in this paper were produced in arrays of 4 sensors in a 2x2 pattern. Doing this provides proof of concept to the idea that multiple sensors can be created at once. Thus the array size of a manufacturing batch of PHFS can be scaled up larger to increase manufacturing output and decrease labor cost significantly.

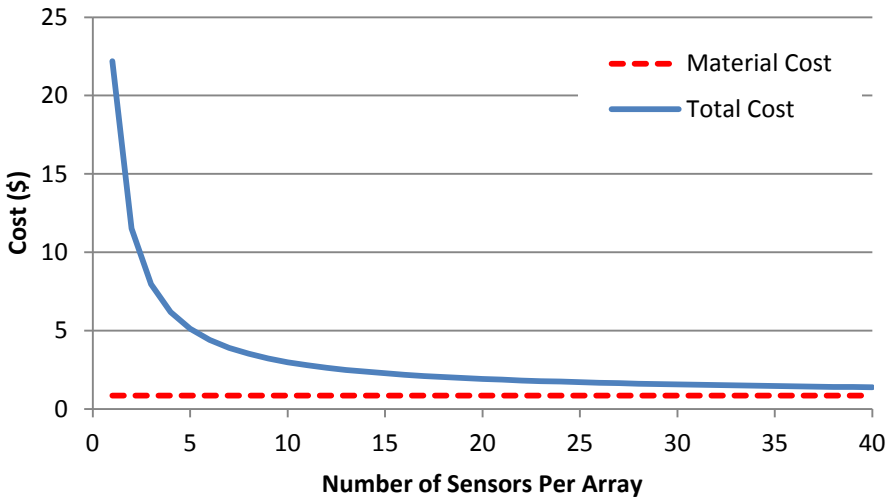

Figure 1.17. Total cost to manufacture the PHFS as a function of number of sensors in an array during a single manufacturing batch.

As seen in Figure 1.17, the cost of manufacturing the PHFS decreases significantly as the number of sensors in an array manufacturing batch is increased. The maximum possible size of the array in a manufacturing batch of PHFS is only limited to the size of the equipment used. The equipment limitations are determined by the maximum copper etching area, laser drilling area, printing stencil size, and box oven size to cure the conductive inks.

2.8.6. Discussion of Results

Table 1.4 describes the compiled performance characteristics of the PHFS along with that of various other heat flux sensors that have been commercially available.

Table 1.4. Compiled performance specifications of various heat flux sensors that have been commercially available and the PHFS.

Heat Flux Sensor	**Sensitivity ($mV/(W/cm^2)$)**	**Response Time (s)**	**Thickness (microns)**	**Cost ($)**
Micro-Foil (Version #1)	0.63 – 34.7	0.02 – 0.4	76 - 330	500 - 835
Episensor	8.35	1.0	350	250
BF Heat Flux Transducer	0.5 – 10	0.9	200	150
Schmidt-Boelter	0.150	0.5	N/A	500 – 1,300
Heat Flux Microsensor	0.150	$17x10^{-6}$	22	2,880
Micro-Foil (Version #2)	8.201	0.13	165	210
Printed Heat Flux Sensor (PHFS)	4.10	0.592	216	7.73

With an average 63% response time of 0.592 s and sensitivity of 4.10 $mV/(W/cm^2)$, the PHFS is comparable to other heat flux sensors that are currently available of similar total sensor thicknesses. The PHFS has a faster response time than the BF heat transducer and the Episensor but is slower than the HFM and RDF Micro-Foil sensors.

The RDF Corporation's Micro-Foil 27160, referenced as version 2 in this paper, is the cheapest currently available thin-film HFS with a cost of $210. The PHFS maintains similar performance characteristics to the Micro-Foil 27160 while being manufactured for 97% less cost. The PHFS also does not encounter the same design issues that the Micro-Foil 27160 does since the PHFS utilizes a direct measurement technique instead of an adjacently located thermocouple pair arrangement.

2.9. Conclusions

The work performed for this paper determined that it is possible to stencil print through vias in 76 micron thick Kapton substrate to produce two-layer, thermopile based, heat flux sensors. Designing a new manufacturing process based on this concept, allowed for semi-automated production of the PHFS and made it possible to manufacture relatively inexpensive heat flux sensors. With an estimated material cost of $0.85, labor cost of $6.18, and assuming a manufacturing yield of 80%, a total cost of $7.73 to produce the PHFS was calculated. With the exception of one outlier sensor in the sample of 12, the manufacturing process was found to be repeatable by consistently producing sensors within 20% of the nominal sensitivity value of 4.10 mV/(W/cm^2). The PHFS nominal sensitivity and response time of 0.592 s showed that it is possible to manufacture heat flux sensors with comparable performance characteristics at a fraction of the price to that of similar commercially available sensors.

2.10. Acknowledgment

This material is based upon work supported by the National Science Foundation under Grant No. 1254006 under the Transforming Undergraduate Education in Science, Technology, Engineering and Mathematics (TUES) program. Any opinions, findings, and conclusions or recommendations express in this material are those of the authors and do not necessarily reflect the views of the National Science Foundation.

2.11. References

1. "Schmidt-Boelter." *Schmidt-Boelter*. Vatell Corporation, n.d. Web. 1 June 2015.

2. Standard test method for measuring heat flux using surface-mounted one-dimensional flat gages, DOI: 10.1520/E2684-09, ASTM International, West Conshohocken, PA, 2009, www.astm.org (ASTM Standard E2684, 2009).

3. Diller, Thomas E. "Chapter 34 Heat Flux." Ed. John G. Webster. *The Measurement, Instrumentation, and Sensors Handbook*. Boca Raton, FL: CRC Published in Cooperation with IEEE, 1999. N. pag. Print.

4. Ewing, Jerrod, Andrew Gifford, David Hubble, Pavlos Vlachos, Alfred Wicks, and Thomas Diller. "A Direct-measurement Thin-film Heat Flux Sensor Array." *Measurement Science and Technology Meas. Sci. Technol*.21.10 (2010): 105201. *Iopscience*. Web. 8 Aug. 2015.

5. Hager, Nathaniel E. "Thin Foil Heat Meter." *Rev. Sci. Instrum. Review of Scientific Instruments* 36.11 (1965): 1564. Web. 7 July 2015.

6. D. G. Holmberg and T. E. Diller, High-frequency heat flux sensor calibration and modeling, ASME. J. *Fluids Eng*., 117, 659-664, 1995.

7. D. J. Ortolano and F. F. Hines, A simplified approach to heat flow measurement. *Advances in Instrumentation*, Vol. 38, Part II, Research Triangle Park: ISA, 1983, 1449-1456.

8. J. P. Terrell, New high sensitivity, low thermal resistance surface mounted heat flux transducer, Proc. 42nd *Int. Instrum. Symp*., Research Triangle Park, NC: ISA, 1996, 235-249.

9. "Vatell BF Datasheet." *Sequoia Technology*. Sequoia Technology, n.d. Web. 9 Sept. 2015.

10. R. L. Hauser, Construction and performance of in situ heat flux transducers, in E. Bales et al. (eds.), *Building Applications of Heat Flux Transducers*, ASTM STP 885, 1985, 172-183.

11. Orlande, Helcio R. B. *Thermal Measurements and Inverse Techniques*. Boca Raton, FL: CRC, 2011. Print.

12. Bomberg, Mark, George E. Courville, and Erv L. Bales. *Building Applications of Heat Flux Transducers: A Symposium Sponsored by ASTM Committee C-16 on Thermal Insulation: (also: Workshop on Building Applications of Heat Flow Sensors); Philadelphia - Pa., 22-23 Sept.1983*. Philadelphia - Pa: ASTM, 1985. Print.

13. Hager JM, Simmons SS, Smith DD, Onishi SS, Langley LW, Diller TE, Experimental Performance of a Heat Flux Microsensor. ASME. J. *Eng. Gas Turbines Power*. 1991;113(2):246-250. DOI:10.1115/1.2906555.

14. J. M. Hager, S. Onishi, L. W. Langley, and T. E. Diller, High temperature heat flux measurements, AIAA J. *Thermophysics Heat Transfer*, 7, 531-534, 1993.

15. Dupont. "Summary of Properties of Kapton Polyimide." [cited 2006; Available from: http://www2.dupont.com/Kapton/en_US/assets/downloads/pdf/summaryofprop.pdf]

16. Jacquot A, Lenoir B, Dauscher A, Stolzer M and Meusel J 2002 Numerical simulation of the 3ω method for measuring the thermal conductivity *J. Appl. Phys.* 91 4733–8.

17. Duby, S., B. Ramsey, D. Harrison, and G. Hay. "Printed Thermocouple Devices." *Proceedings of IEEE Sensors*, 2004. (2004): n. pag. Web.

18. Taylor, B.N. and C.E. Kuyatt, "Guidlines for Evaluating and Expressing the Uncertainty of NIST Measurement Results." 1994, Physics Laboratory, *National Institute of Standards and Technology*: Gaithersburg, MA.

19. Pullins, C.A., High temperature heat flux measurement: sensor design, calibration, and applications, *Virginia Tech Dissertation* (2011) 120.

Chapter 3: Conclusions and Recommendations

3.1. Conclusions

The work performed for this paper determined that it is possible to stencil print through vias in 76 micron thick Kapton substrate to produce two-layer, thermopile based, heat flux sensors. Designing a new manufacturing process based on this concept, allowed for semi-automated production of the PHFS and made it possible to manufacture relatively inexpensive heat flux sensors. With an estimated material cost of $0.85, labor cost of $6.18, and assuming a manufacturing yield of 80%, a total cost of $7.73 to produce the PHFS was calculated. With the exception of one outlier sensor in the sample of 12, the manufacturing process was found to be repeatable by consistently producing sensors within 20% of the nominal sensitivity value of 4.10 $mV/(W/cm^2)$. The PHFS nominal sensitivity and response time of 0.592 s showed that it is possible to manufacture heat flux sensors with comparable performance characteristics at a fraction of the price to that of similar commercially available sensors.

3.2. Recommendations for Future Work

Through the course of performing the research and testing presented in this paper certain limitations in the PHFS were found that could be mediated with further development of the manufacturing process and PHFS design. It was found that the conductive inks are not able to make perfectly stable connections through the vias especially when the sensors are bent a significant amount. The silver ink connections could be taken out of the sensor entirely if the silver ink via holes are copper plated instead of being printed through. Copper plating via holes is a proven method of making stable connections between flexible circuit layers. Using copper plating would change the manufacturing process order but it would only leave half of the ink to

copper connections where electrical instability may be occurring during flexion. Copper bulk material also has a similar Seebeck coefficient to that of the silver conductive ink so PHFS sensitivity would not decrease.

Alternative conductive ink materials could also be investigated to find materials with larger absolute Seebeck coefficients. Commercially available inks are largely limited to silver and carbon based inks, both of which have a positive Seebeck coefficient. Work done by Duby et al. [17] proved it was possible to print single layer thermoelectric devices with bismuth/antimony inks. Research could be continued to determine whether these semiconductor inks can be used to print through vias to provide stable interlayer electrical connection. If it is possible, then the ink thermocouples would have a Seebeck coefficient approximately a magnitude larger than those tested in this paper. Thus a printed sensor of the same size could be made with a magnitude larger sensitivity or a sensor of the same sensitivity could be made much smaller using one order-of-magnitude fewer thermocouple junctions.

Additional work can be made in finding alternative encapsulation methods to electrically insulate the heat flux sensor circuit from the surroundings. The current method is to adhere Kapton tape to either side of the sensor. While the Kapton tape is only 25.4 microns thick, the silicon adhesive is specified to be 50.8 microns thick. Adding 152.4 microns of tape for encapsulation compared to approximately 177.8 microns of sensor thickness nearly doubles the total thickness. A thinner and more thermally conductive encapsulation method would make the sensor more accurate, less thermally resistant, and provide a smaller profile for convective heat measurements.

It was noticed that flexing the PHFS greater than a 90 degree bend would occasionally compromise the electrical connections between the conductive inks and the copper jumper

traces. Therefore a great deal of care was necessary in handling the PHFS especially during mounting or unmounting the sensor to a surface. For this reason it is recommended that the current design of the PHFS be permanently mounted to the measurement surface using a thin layer of adhesive for conducting measurements. If it is necessary to remove the sensor at any point it can be ripped off and replaced since the PHFS is relatively inexpensive. Alternatively, an additional more rigid encapsulation material can be used to limit the range of flexion possible for the PHFS. A metal material such as aluminum would be most appropriate since it is highly thermally conductive and relatively rigid in thin sheets.

Manual stencil printing performed to manufacture the sensors tested in this paper is an acquired skill by the user. Automated screen printing systems can be implemented to print the conductive inks through the via holes. Automated printing systems are able to print up to 1200 times per hour and also consistently use the same squeegee parameters such as pressure and tilt angle. With these capabilities, the manufacturing output and yield would be significantly higher while also making performance characteristics more consistent from sensor to sensor.

Stencil printing for this paper used a 76.2 micron thick Kapton material as the stencil mask. The mask was held taught by adhering it tightly to a frame. If this adhesion was not done very well the alignment of the mask would change and the quality of the printed sensors would decrease. It is recommended that a metal stencil of similar thickness be used for providing the mask during printing of the conductive inks. A metal stencil will remain rigid and could also provide outer alignment holes so quality of the PHFS will be consistently acceptable.

Appendix A: Detailed Manufacturing Process of the PHFS

This appendix shows a detailed step by step process used to manufacture the PHFS. It includes preparation of equipment and material that is only required to be done once and then also the process necessary during manufacture of each batch of PHFS's.

A.1. Preparation of Manufacturing Materials and Equipment

This process is performed once to prepare materials required for manufacture the PHFS. These steps should not have to be repeated unless the design/layout of the PHFS is changed

1. Design of the sensor is created on a vector based illustration computer program by specifying desired parameters. The dimensioned designs for the copper jumper traces are shown in Figure A.1.

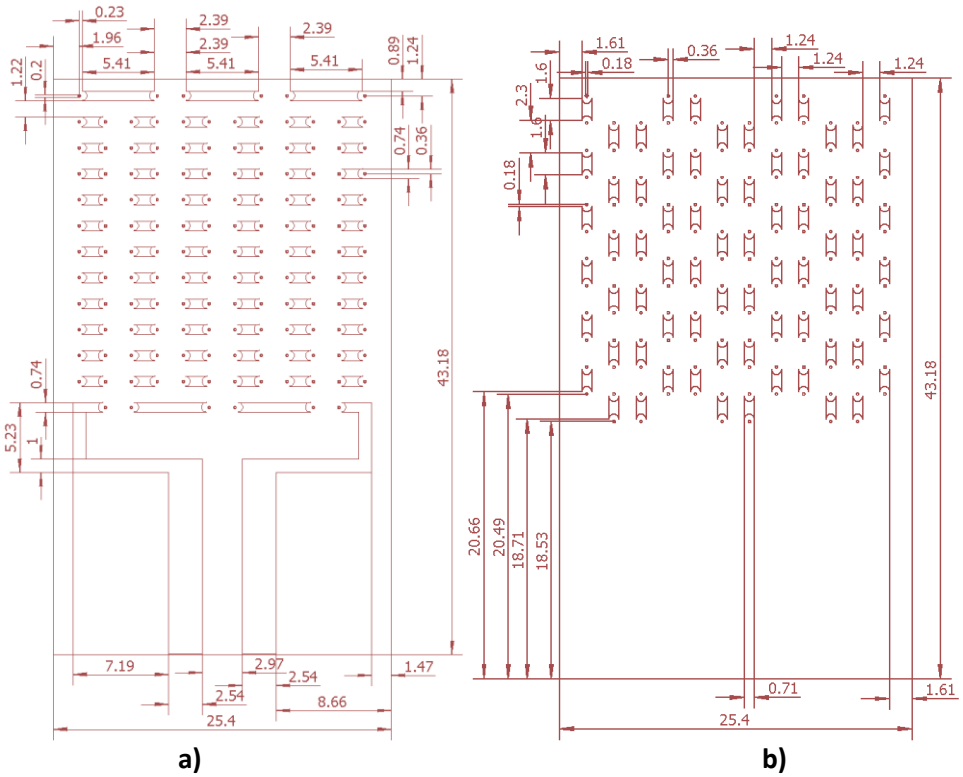

Figure A.1. Dimensioned diagrams of the copper jumper traces on the **a)** top and **b)** bottom surfaces of the polyimide Kapton TRL substrate.

2. A stencil for each the bottom and top layer copper trace patterns is laser cut into an opaque acrylic sheet to be used as mask during the copper etching process using a V-460 50W CO_2 laser cutting system with the following settings: Vector graphic, 60% power, 10% speed, 1000 ppi.
3. Sensor design is broken up into each material portion and designed using a vector based illustrator program such as CorelDraw. The dimensioned printing masks are pictured in Figure A.2.

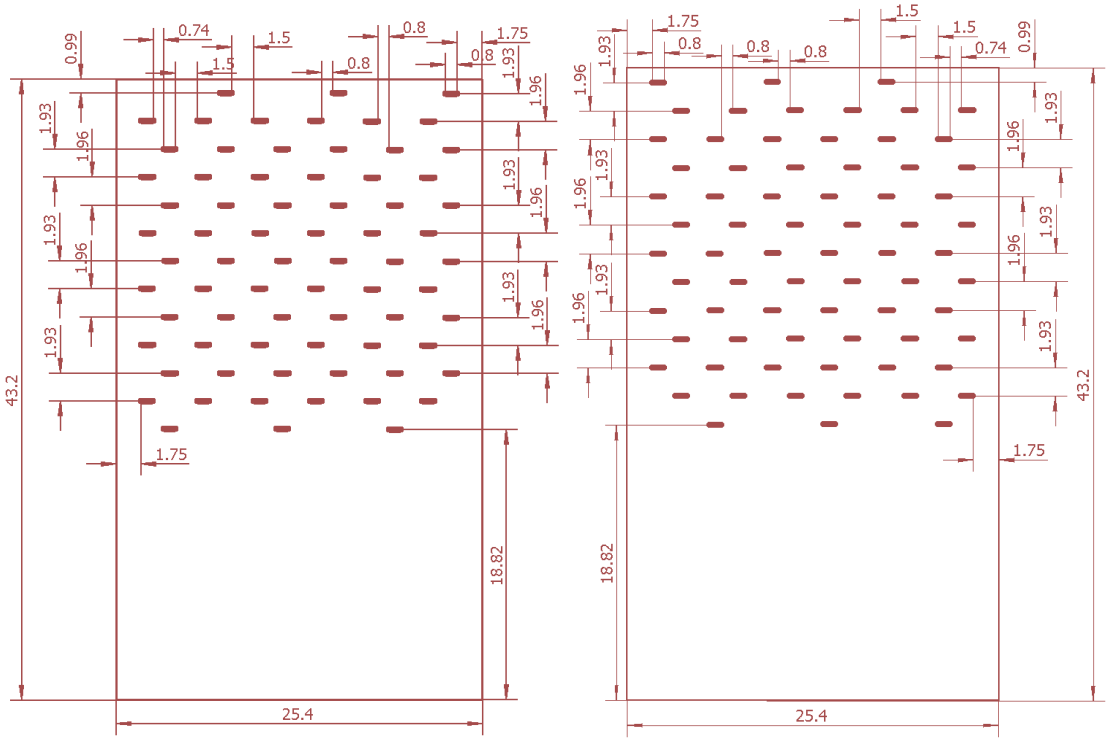

Figure A.2. Dimensioned diagrams of the two printing stencil masks used to pattern the **a)** silver and **b)** nickel conductive ink thermopile materials on the top surface of the polyimide Kapton TRL substrate.

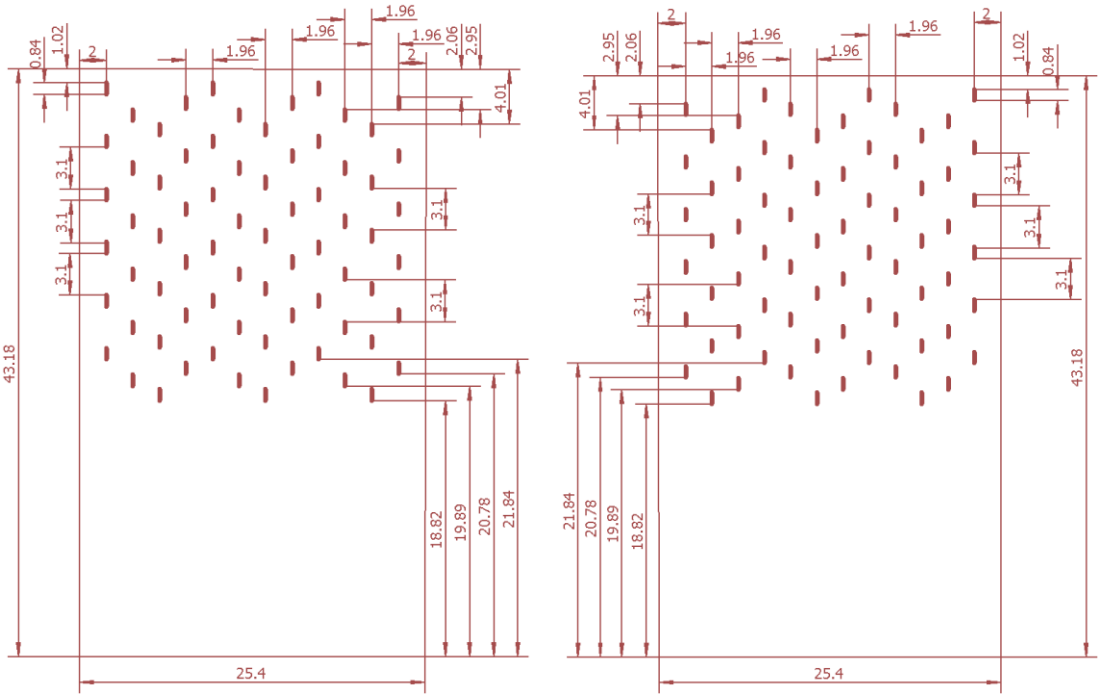

Figure A.3. Dimensioned diagrams of the two printing stencil masks used to pattern the **a)** silver and **b)** nickel conductive ink thermopile materials on the bottom surface of the polyimide Kapton TRL substrate.

4. The four stencil masks are cut into 76.2 micron thick Kapton film for each of the conductive ink patterns using a V-460 50W CO_2 laser cutting system with the following settings: Raster graphic, 13% power, 5% speed, 1000 ppi. (Top surface EMS CI-1001 silver ink, bottom surface EMS CI-1001 silver ink, top surface EMS CI-5001 nickel ink, bottom surface EMS CI-5001 nickel ink).
5. The four Kapton stencil masks are held taught and attached to frames for ease of printing.

A.2. Manufacturing Process of the PHFS

These steps are performed every time a batch of PHFS is manufactured.

1. Pyralux AP 9131R is laminated with a dry photoresist film on both the top and bottom surface.

2. The opaque acrylic stencil masks are pressed tightly against both surfaces of the substrate
3. A light source is used to cure the portions of the dry photoresist film that is exposed through the holes in the opaque acrylic mask.
4. The cured dry photo resist is developed while the uncured dry photoresist is removed by rinsing the substrate with sodium carbonate developing solution for approximately 3 minutes.
5. The entire substrate is placed into ferric chloride. The copper clad that is not protected by the cured dry photoresist is etched away. Once complete the only remainder is the patterned copper traces and the underlying polyimide Kapton substrate.
6. 180 micron diameter electrical vias are drilled through the polyimide Kapton substrate using a V-460 50W CO_2 laser cutting system with the following settings: Raster graphic, 13% power, 5% speed, 1000 ppi.
7. The conductive inks are agitated to ensure even dispersion of metal particles within the polymer carrier and solvent mixture.
8. The printing stencil with the pattern corresponding to the CI-1001 silver ink top surface design is aligned over the substrate.
9. A portion of CI-1001 silver ink is doctor bladed across the stencil so that the voids in the stencil pattern is filled with the conductive ink.
10. The printing stencil is removed and the ink is thermally cured in an oven at 130°C for 10 minutes.
11. Steps 7-10 are repeated 3 times for printing CI-1001 silver ink on the bottom surface as well as CI-5001 nickel ink on the top and bottom surfaces.

12. A copper wire lead is soldered to each of the voltage measurement locations for heat flux voltage measurements. A constantan wire lead is also soldered to one of the locations for an added temperature measurement.
13. The entire thermopile circuit is encapsulated with a 25.4 micron thick polyimide kapton adhesive tape.

Appendix B: Estimation of Uncertainty in Calculations/Measurements

This appendix is used to estimate the uncertainty in the various calculations and measurements performed in this thesis. The National Institute of Standards and Technology (NIST) Technical Note 1297 Guidelines for Evaluation and Expressing the Uncertainty of NIST Measurement Results [18] was used as a guide for determining the uncertainty values for Seebeck measurements, radiation calibrations, conduction calibrations, time response measurements.

B.1. Seebeck Coefficient Uncertainty

The uncertainty of calculating the Seebeck coefficient of the nickel/silver conductive ink thermocouple materials comes from the following equation B.1

$$Se = \frac{\Delta V}{\Delta T} = \frac{\Delta V}{(T_1 - T_2)} \tag{B.1}$$

where ΔV is the induced voltage by the thermocouple material at the measurement points and ΔT is the temperature differential experienced by the thermocouple from the junction to the voltage measurement points. T_1 is the temperature measurement at the thermocouple junction while T_2 is that at the measurement point. The potential sources of uncertainty arise from the voltage measurement for the term ΔV and the two independent type-T thermocouple temperature measurements T_1 and T_2 used to form ΔT. Using the law of propagation of uncertainty equation B.2 is formed to calculate the total uncertainty, u_c in the Seebeck coefficient measurement

$$u_c = \sqrt{\left(\frac{\partial Se}{\partial V}\right)^2 u_V^2 + \left(\frac{\partial Se}{\delta T_1}\right)^2 u_{T_1}^2 + \left(\frac{\partial Se}{\partial T_2}\right)^2 u_{T_2}^2} \tag{B.2}$$

where u_v is the uncertainty in the tested thermocouple output voltage measurement by the DAQ which is 2.2 μV. u_{T1} is the uncertainty in the type-T thermocouple measuring the heated test thermocouple junction temperature, and u_{T2} is the uncertainty in the type-T thermocouple

measuring the unheated room temperature voltage leads. The uncertainty in type-T thermocouples is 1.0 °C. The partial derivatives are known as the sensitivity coefficients and are evaluated using equation B.1 to form the final combined uncertainty equation B.3

$$\frac{u_c}{Se} = \sqrt{\left(\frac{1}{V}\right)^2 u_V^2 + \left(\frac{1}{T_1}\right)^2 u_{T_1}^2 + \left(\frac{1}{T_2}\right)^2 u_{T_2}^2} \tag{B.3}$$

The uncertainty budget for the various sources of error is listed in Table B.1 and used in a Matlab program to calculate the combined uncertainty for each measurement taken during a Seebeck coefficient data run.

Table B.1. Uncertainty budget while measuring Seebeck coefficient.

Source of Uncertainty	**Standard Value of Uncertainty**
9214 NI-DAQ Voltage Measurement	2.2 μV
Type-T Temperature Measurement T_1	1.0 °C
Type-T Temperature Measurement T_2	1.0 °C

The uncertainties for each measurement are averaged for that data run then the data run averages were averaged together to get a final uncertainty value of 0.9 uV/°C for Seebeck coefficient testing.

B.2. Radiation Sensitivity Calibration Uncertainty

The uncertainty of calculating the sensitivity of the PHFS using the radiation calibration system comes from the following equation B.4

$$S_{PHFS} = \frac{V_{PHFS}}{q''_{absorbed}} \tag{B.4}$$

where S_{PHFS} is the sensitivity of the PHFS, V_{PHFS} is the output voltage of the PHFS, and $q''_{absorbed}$ is the absorbed heat flux as determined by prior system calibration using the Schmidt-Boelter reference gage. The potential sources of uncertainty arise from the voltage measurement of the

PHFS heat flux voltage output by the DAQ and the uncertainty in the Schmidt-Boelter reference heat flux measurement. Using the law of propagation of uncertainty equation B.5 is formed to calculate the total uncertainty, u_c in the PHFS sensitivity measurements while using the radiation calibration system.

$$\frac{u_c}{S_{PHFS}} = \sqrt{\left(\frac{1}{V_{PHFS}}\right)^2 u_{V_{PHFS}}^2 + \left(\frac{1}{q"_{SB}}\right)^2 u_{q"_{SB}}^2} \tag{B.5}$$

Uncertainty in the initial calibration of the radiation calibration system using the Schmidt-Boelter gage is combined together to determine $u_{q"SB}$. To find this uncertainty the initial calibration measurements are investigated and shown equation B.6.

$$S_{SB} = \frac{V_{SB}}{q"_{absorbed}} \tag{B.6}$$

where S_{SB} is the known sensitivity of the Schmidt-Boelter gage, V_{SB} is the voltage output of the SB gage and $q"_{absorbed}$ is the absorbed heat flux by the SB gage. Since the absorbed heat flux is a function of the supplied lamp voltage, $V_{supplied}$, equation B.6 is rewritten as equation B.7 for uncertainty analysis.

$$S_{SB} = \frac{V_{SB}}{V_{supplied}} \tag{B.7}$$

Uncertainty of the supplied lamp voltage is the resolution of the HP 3468A multimeter VAC measurement reading of 0.1 mV. Measuring the Schmidt-Boelter heat flux output voltage using the 9214 DAQ system has an uncertainty of 2.2 μV. The uncertainty budget for the various sources of error is listed in Table B.2 and used in a Matlab program to calculate the combined uncertainty for each measurement taken during a radiation calibration data run.

Table B.2. Uncertainty budget for measuring PHFS sensitivity using the radiation sensitivity calibration system.

Potential Source of Uncertainty	**Value of Uncertainty**
9214 DAQ Voltage Measurement	2.2 μV
Schmidt-Boelter Reference Sensor	3% of measured q"
Initial Radiation System Calibration: DAQ Voltage measurement HP 3468A multimeter input voltage measurement	 2.2 μV 0.1 mV

The uncertainties for each measurement are averaged for that data run then the data run averages were averaged together to get a final uncertainty value of 0.13 mV/(W/cm^2) for radiation calibration testing.

B.3. Conduction Sensitivity Calibration Uncertainty

The uncertainty in calculating the sensitivity of the PHFS, S_{PHFS}, using the conduction calibration system originates from the following equation B.6

$$S_{PHFS} = \frac{V_{PHFS}}{q"} = \frac{V_{PHFS} S_{ref}}{V_{ref}} \tag{B.6}$$

where V_{PHFS} is the voltage output of the PHFS, q'' is the absorbed heat flux through the PHFS. This absorbed heat flux is determined from the RDF Model-27170 reference heat flux sensor with sensitivity S_{ref} and output voltage V_{ref}.

Using the law of propagation of uncertainty equation B.7 is formed to calculate the total uncertainty, u_c in the PHFS sensitivity measurements while using the conduction calibration system.

$$\frac{u_c}{S_{PHFS}} = \sqrt{\left(\frac{1}{V_{PHFS}}\right)^2 u_{V_{PHFS}}^2 + \left(\frac{1}{q"_{ref}}\right)^2 u_{q"_{ref}}^2 + \left(\frac{1}{V_{ref}}\right)^2 u_{V_{ref}}^2} \tag{B.7}$$

The uncertainty budget for the various sources of error is listed in Table B.3 and used in a Matlab program to calculate the combined uncertainty for each measurement taken during a conduction calibration data run.

Table B.3. Uncertainty budget for measuring PHFS sensitivity using the conduction sensitivity calibration system.

Potential Source of Uncertainty	**Value of Uncertainty**
9214 DAQ Voltage Measurement for V_{PHFS}	2.2 µV
RDF Reference HFS Heat Flux Value	4% of measured q”
9214 DAQ Voltage Measurement for V_{ref}	2.2 µV

The uncertainties for each measurement are averaged for that data run those were averaged together to get a final uncertainty value of 0.23 mV/(W/cm^2) for conduction calibration testing.

B.4. Time Response Uncertainty

The time response of the PHFS was evaluated by analyzing transient voltage signals output from the PHFS measured by the 9214 NI-DAQ system. A step input is induced onto the PHFS sensor by removing an opaque shutter at a rate of 20 m/s to expose a radiative heat source supplied by halogen lamps. The radiative heat travels through a bore size of 5.70 cm in diameter in the water cooled radiation calibration system. While the shutter is being removed, there is a period of 2.9 ms that the PHFS is exposed to a fraction of the full step input.

A Matlab program is used to determine at what times in which the step input is started, t_0, and when the PHFS voltage output reached 63% of the final averaged steady state output, $t_{63\%}$. The difference in these values is the time response of the PHFS, t_r,. The uncertainty of calculating the time response using the radiation calibration system comes from the following equation B.8.

$$t_r = t_{63\%} - t_0 \tag{B.8}$$

Using the law of propagation of uncertainty equation B.9 is formed to calculate the total uncertainty, u_c, in the time response measurement.

$$\frac{u_c}{t_r} = \sqrt{u_{63\%}^2 + u_0^2} \tag{B.9}$$

where $u_{63\%}$ is the uncertainty in the time measurement for 63% of final PHFS voltage output and u_0 is the uncertainty in determining the time of initiation of the step input. The uncertainty in the measurement of $t_{63\%}$ originates from the time measurement resolution of the DAQ which is set to sample at 75 Hz or resolution time of 13.33 ms. Also contributing to uncertainty in $t_{63\%}$ is the time of 2.9 ms in which the shutter exposes the PHFS to only a fraction of the step input radiative heat flux. The root of the squares is taken of these two uncertainties to calculate $u_{63\%}$ to equal 13.64 ms.

The uncertainty in the measurement of t_0 is due to a combination of the time measurement resolution of the DAQ and the researcher's capability to determine an accurate initiation time for the step input. The resolution of the DAQ is 13.33 ms originating in the 75 Hz sample rate. From testing it was found easily possible to determine the step input initiation time within three samples or 40 ms at 75 Hz. Combing these two uncertainties together by rooting the sum of squares results in an uncertainty, u_0, value of 42.16 ms. The uncertainty budget for the various sources of error is listed in Table B.4 and used in a Matlab program to calculate the combined uncertainty for each measurement taken during a time response data run.

Table B.4. Uncertainty budget for PHFS time response measurements.

Potential Source of Uncertainty	Value of Uncertainty
Measurement of t_0:	
DAQ time resolution	13.33 ms (75 Hz)
User selection of t_0 in Matlab	40 ms
Measurement of $t_{63\%}$:	
DAQ time resolution	13.33 ms (75 Hz)
Initiation of step input	2.9 ms

The total uncertainty of each data run was calculated and then averaged together to determine that the combined uncertainty in the time response data for the PHFS is 0.026 s.

Appendix C: Conduction Sensitivity Calibration Procedure

Sensor calibration can be performed using means of conduction heat transfer. This appendix describes the equipment, programs, and step by step process necessary to perform a conduction calibration on a PHFS.

C.1. Necessary Equipment for Conduction Sensitivity Calibration

1. NI-DAQ 9214 24-bit Delta-Sigma A/D
2. Dell laptop
3. Reference thin-film heat flux sensor (RDF Micro-Foil Model 27170-2: Serial Number = 13120741) used during testing in this paper.
4. PHFS to be calibrated.
5. Ice in bucket used to decrease cooling water temperature
6. Hewitt-Packard 6200B DC power supply with 0V to 50V DC voltage range
7. Conduction calibration setup
    a. Gap pads (2)
    b. Resistance heating unit
    c. Water cooled metal plate
    d. Water pump with water supply
    e. Metal weight
    f. Two Kapton masks each matching the thickness of each sensor used

C.2. Conduction Sensitivity Calibration System Hardware Set Up Procedure

1. Make sure the conduction calibration system is on a steady, level surface.

2. Attach the positive and negative heat flux voltage leads of the reference RDF Micro-Foil Model 27170-2 to the 24-bit NI-DAQ 9214 in channel 0.
3. Attach the positive and negative heat flux voltage leads of the PHFS to the 24-bit NI-DAQ 9214 in channel 1.
4. Plug in or connect the leads of the resistance heating unit to a voltage power supply regulator.
5. Place a gap pad, that is equal to or larger than the size of the resistance heating unit, on top of the heating unit.
6. Place the reference RDF HFS sensor on top of the gap pad.
7. Place a Kapton mask that is of equal thickness as the reference RDF sensor around the RDF sensor. The mask should be cut with a gap in the middle to the dimensions of the RDF HFS so that there is minimal space lateral space between the RDF sensor and the Kapton mask. The Kapton should also extend out farther than the dimensions of the heating unit.
8. Place the PHFS on top of the RDF reference sensor making sure to align the sensing areas directly on top of one another. If the size of the PHFS is smaller than that of the dimensions of the resistance heating unit an additional Kapton mask is required with the same requirements to be placed around the PHFS.
9. Add another gap pad on top of the stacked sensors.
10. Lower the water cooled metal plate to compress the two stacked sensors, mask(s), and gap pads.

11. Compress the assembly further by placing the large metal weight on top which is designed to provide even weight distribution. The weight compresses the sensors tightly together, thus making minimal and uniform thermal contact resistance.

C.3. Determining Measurement System Voltage Offset

1. Without the cooling water pumps running or any voltage supplied to the resistance heating unit begin a data run using LabVIEW.
2. The reported voltage from each of the heat flux sensors should be a value corresponding for zero heat flux. Theoretically the voltages reported from the sensors should be zero volts for zero induced heat flux. The NI-DAQ systems use operational amplifiers within their internal circuits to amplify signals. Inherently within operational amplifiers there is an input current bias. This input current bias is approximately 0.2 μA for the NI 9214 DAQ. Therefore if a sensor is 2 kΩ internal resistance, the DAQ will report a 400 μV offset which could significantly affect measurements.

$$V_{offset} = I_{offset} R_{internal} = (0.2\ \mu A)(2000\ \Omega) = 400\ \mu V \qquad \text{(C.1)}$$

3. Take at least two minutes of data using LabVIEW with zero induced heat flux and average it together to get the voltage offset. Record this offset value since it is a constant regardless of sensor conditions and will be subtracted from all future measurements.

C.4. Performing a Conduction Sensitivity Calibration Run

1. Open the LabVIEW program named ‘Conduction_Calibration’

2. Start water pumps and start supplying the resistance heater with a low voltage BEFORE beginning a data run. (This will insure that any measurements will be taken at heat fluxes larger than zero to avoid mathematical problems of dividing by zero).
3. Begin recording data using the LabVIEW program. The program simultaneously measures output voltages of both the reference RDF sensor and the PHFS being calibrated.
4. Vary the heat flux through a wide range from about 50 W/m^2 up to over 2000 W/m^2 by either increasing the supplied voltage to the resistance heater and/or decreasing the temperature of the water pumped to the cooling plate.
5. Once a wide range of heat fluxes has been measured, stop the LabVIEW program to cease recording data.

C.5. Analyzing the Measured Conduction Sensitivity Calibration Data

1. Open Matlab and the Matlab code named 'Conduction_Calibration.m' found in Appendix E.
2. Ensure that the sensitivity and voltage offset values for the reference RDF HFS is correct. The values used for the RDF reference sensor (Model 27170-2: Serial Number=13120741) used for testing in this paper are S=18.703 (mV/(W/cm^2)) and V_{offset}=37.66 μV.
3. Run MatLab program, the reported value is the PHFS sensitivity. The program uses measured PHFS voltage values, RDF sensor values and known RDF sensor sensitivity to calculate PHFS sensitivity according to the following formula

$$S_{PHFS} = \frac{V_{PHFS} S_R}{V_R} \tag{C.2}$$

Where V_{PHFS} is the output voltage of the printed heat flux sensor, S_R is the sensitivity of the reference heat flux sensor, and V_R is the voltage output of the reference heat flux sensor.

4. Plots the PHFS output voltage as a function of measured heat flux from the reference RDF sensor.

Appendix D: Radiation Sensitivity Calibration Using Lamp

This appendix serves as a guideline for all heat flux gauge lamp calibrations in 100V. It is best to try and follow these procedures to ensure consistent calibration methods are being used [19].

D.1. Necessary Equipment for Radiation Sensitivity Calibration

Halogen Lamp:

- USHIO J120V-250W/79 halogen bulbs
- Life of 2000 hours
- Lamp has focal point of 1.25" away from its face

Model SC-10T Variac:

- 0-130 VAC
- Max 1000W
- 117VAC, 60 Hz input

HP 3468A True RMS Multimeter:

- We want to measure AC

PHFS and SB gauge with holders:

- Each has their own plate holder. We want to figure this out.
- SB gauge has sensitivity of 625.19 uV/(W/cm^2). It is used to calibrate the lamp.

Gage Holster:

- Same gage holster used for both SB and PHFS

NI cDAQ 9172:

- 24 bit Sigma delta A/D

- 9213 thermocouple module
- 9219 voltage module
- PHFS temperature lead, water temp lead

Dell laptop

- Has the necessary LabVIEW files on it

Ice in a bucket

- To regulate coolant temperature

D.2. Experimental Setup for Radiation Sensitivity Calibration

1. Gather all needed equipment.
2. Configure the lamp and the gage holster facing towards each other.
3. Connect water hoses to lamp.
    a. This requires that two hoses are connected to the water pumps and then to one side of the lamp (provide cooling water). Another two hoses are connected to the other side of the lamp and are allowed to empty into the water bin (take cooling water away).
4. Connect water hoses to gauge.
    a. For the SB gauge, there are 4 hoses total. Two hoses should be hooked up to one pump to provide cooling water to both the gage and the plate. The other two hoses are free to the bin to take the cooling water away from both the gauge and the plate.
    b. For the PHFS, there are 5 hoses. One hose provides cooling water to the gage and is thus connected to a pump while all other hoses are free to the water bin.

5. Mount gauge into plate holder. Use double sided adhesive tape uniformly across the back surface of the sensor and press firmly to the plate holder.
6. Mount gauge and holder into gauge holster. Use machinist ruler to ensure gage face is 1.25" away from lamp face. Tighten bolts on holster so that it becomes fixed to lamp base (does not move/wiggle).
7. Plug in lamp and multimeter to variac (brown to red and blue to black). Make sure multimeter and variac are also plugged in.
8. Connect all lead wires to DAQ (See Figure 1).
    a. SB gage lead wires are white (+) and black (-). These leads go connected to the 9219 module. Connect the leads to any desired channel but ensure that the white wire (+) is connected to terminal 4 (high signal) and the black wire (-) is connected to terminal 5 (low signal).
    b. For the PHFS, the blue copper wires are the voltage leads for heat flux measurement. For temperature measurements, the copper blue lead is positive (+) type – T, and the constantan red wire is (-) type-T. When connecting connectors together, positive side goes to positive and negative goes to negative. These go connected to the 9213 module for temperature readings and then connected to the 9219 for heat flux readings. See figure below for setup.
    c. Make sure to connect a TC for the water temp.
9. Configure Labview file to read channels as they are hooked up and for a sampling rate of 1Hz.

10. To do this, open the Labview file titled “PHFS Radiation Calibration” or “SB Radiation Calibration” depending on which you are performing. Open the DAQ Assistant block and ensure that the physical channels correspond to the actual channel.
11. You are now ready to calibrate.

D.3. Radiation Sensitivity Calibration Procedure

1. Turn on DAQ and allow warm up of 15 min.
2. Check to make sure all hoses are connected properly.
3. Check that all lead wires are connected properly.
4. Check to make sure VI channels correspond to actual channels.
5. When the system is at thermal equilibrium with the surroundings (Before water pumps or heater are turned on) run the VI to make sure text file of raw data is being written.
6. Collect data at thermal equilibrium for at least 2 min prior to ramping up the voltage. This is the voltage offset in the system and will be subtracted off of the data (Subtracting bias).
7. Ramp up the voltage on the variac to desired setting and allow for entire system to reach steady state (no change in temperature >0.2 C for 5 min). Repeat for desired voltage levels.
    a. Note: The voltage level is entirely up to the calibrator, however 5 measurements in the range of 40-120V should be fine. We expect the response to be approximately linear to the input voltage.
8. Record all voltage levels. These will be used later in the code.

9. Be sure to monitor the water temperature. If it rises above room temp (22-26 C), add ice to the water bin. It is important to keep the gauge close to room temperature to ensure that convection is kept to a minimum level.

D.4. Radiation Sensitivity Calibration Data Post Processing

This can be done in Excel or Matlab.

<u>For SB:</u>

If you are using the SB gauge to calibrate the lamp, you will

1. Average the baseline measurements (first 2 min) and subtract this average from all of the voltage output data. This gets rid of offset voltage.
2. Go through data and identify the end time of the steady state events.
3. Average the steady state data (example: the end of the steady state event was at 500 seconds so I am going to average the last 60 measurements from 440 to 500).
4. Multiply this by 10^6 to put data into micro-Volts (uV).
5. Take this and divide by the sensitivity (625.19 uV/(W/cm^2)) to get *absorbed* heat flux (heat flux absorbed by sensor).
6. We can now calculate the *incident* heat flux to the sensor by dividing by the emissivity which is 0.94 for the black paint in the lab. (Recall our assumption of negligible convection.)
7. Plot the input voltage versus the incident heat flux. Use a 4^{th} degree polynomial fit to find the coefficients we will use to relate input voltage to incident heat flux for future calibrations.

For PHFS:

If you are calibrating a PHFS, you will

1. Average the baseline measurements (first 2 min) and subtract this average from all of the voltage output data. This gets rid of bias voltage.
2. Go through data and identify the end time of the steady state events.
3. Average the steady state data (example: the end of the steady state event was at 500 seconds so I am going to average the last 60 measurements from 440 to 500).
4. Multiply this by 10^6 to put data into micro-Volts (uV).
5. Use the coefficients from the SB calibration and evaluate the polynomial equation at the voltage levels used during the calibration. This gives the *incident* heat flux of the lamp.
6. We can now calculate the *absorbed* heat flux to the sensor by multiplying by the emissivity which is 0.94 for the black paint in the lab. (Recall our assumption of negligible convection.)
7. Divide the mean SS voltage output from the gage by the absorbed heat flux to get sensitivities in uV/(W/cm^2).

Appendix E: Programming Code Used for Data Collection/Analysis

This appendix is a compilation of the programming code used to analyze the data collected in various tests to determine conductive ink Seebeck Coefficient and PHFS sensitivity.

E.1. MatLab Code Used to Analyze Seebeck Coefficient Data

The following MatLab code was used to analyze the data collected during experimental testing of Seebeck coefficient for a single printed thermocouple made of CI-1001 silver ink and CI-5001 nickel ink.

```
clear all; clc; close all;
data=load('E:\Seebeck_Coefficient\NickelSilver_sample##_run_##.lvm');
time=data(:,1);
Thot=data(:,2); %heated thermocouple junction location temperature
Tcold=data(:,3);  %room temp thermocouple voltage measurement location temperature
Volts=data(:,4); %thermocouple output voltage
%%
microVolts=Volts.*1000.*1000; %convert volts to microvolts
deltaT=(Thot-Tcold);  %calculates temperature differential
fit1=polyfit(deltaT,microVolts,1); %linear least squares regression fit to determine Seebeck

%%
%Plots thermocouple output voltage as a function of temperature
%differential
%slope of the relationship is Seebeck coefficient of the thermocouple
figure(1)
plot(deltaT,microVolts,'linewidth',2)
xlabel('Temperature Differential (C)')
ylabel('Thermocouple Output Voltage (V)')
```

E.2. MatLab Code Used to Analyze Conduction Sensitivity Calibration Data

The following Matlab code was used to analyze the data collected during PHFS sensitivity calibration using the conduction sensitivity calibration system.

```
close all; clear all; clc; %clears matlab program
file='E:\Conduction_Calibration\Conduction_Calibration_sensor##_run_##.lvm';
fid=fopen(file); %open filepath specified previously
num_cols=3; %number of columns in raw data file
a=fscanf(fid, '%f',[num_cols, inf]);
A=a';        %Transposes data set
fclose(fid);

time=A(:,1);
rdfV=A(:,2)*1000*1000;  %takes reference RDF voltage measurements and converts them to
microVolts
PHFS_V=A(:,3)*1000*1000; %takes PHFS voltage measurements and converts them to
microVolts
%temp=A(:,4); %optional PHFS temperature measurement using an additional constantan wire
lead

%%Starting from off
rdfV_offset=37.663413246753244; %measured RDF reference HFS microVoltage offset
rdfV_1=rdfV-rdfV_offset; %subtracts RDF voltage offset from all RDF heat flux voltage
measurements
rdf_S=1.8703;  %RDF reference sensitivity in uV/(W/m^2)
rdfQ_1=rdfV_1./rdf_S;  %Converts reference RDF voltage measurements to heat flux using the
reference sensitivity
format long
S1=polyfit(rdfQ_1,PHFS_V,1);  %Linear regression fit to PHFS voltage as a function of
measured heat flux from reference RDF sensor
PHFS_S=S1(1)  %Reports the slope of the linear fit which is the PHFS sensitivity
PHFS_Voffset=S1(2);   %PHFS voltage offset
PHFS_V_1=(PHFSV-PHFS_Voffset);   %subtracts the PHFS voltage offset from the PHFS
voltage measurements (not necessary for sensitivity calculations)

% %plots
figure(1) %Plots PHFS voltage as a function of heat flux as well as the linear fit regression line
title('PHFS Sensitivity According to RDF Reference')
plot(rdfQ_1,PHFS_V_1)
hold on
plot(rdfQ_1,S1(1).*rdfQ_1,'r')
xlabel('RDF Heat flux (W/m^2)')
ylabel('sensor voltages (microV)')
legend('PHFS','Theoretical')
```

E.3. MatLab Code Used to Analyze Radiation Sensitivity Calibration Data

The following MatLab code was used to analyze data collected during calibration using the radiation calibration system.

```
%%Radiation Calibrations: Halogen lamp characterization
close all; clear all; clc;
eg=0.94; %sensor surface emissivity (coated with Aervoe Z635 Black Zynolyte Hi-Temp spray paint)
%% load data file(s) ----------------------------------------------------------------------------------------------------%%
A=load('C:\Radiation_Calibration\PHFS_sensor##_run##.lvm'); %filepath of data file record from LabVIEW
time=A(:,1);
PHFS_V=A(:,2);
%remove sensor voltage bias
PHFS_Voffset=mean(PFHFS_V(1:120));
PHFS_V1=PHFS_V-PHFS_Voffset;

%individual test conditions
ss=[432 580 713 834 971 1211];  %start measurement sample number for each steady-state heat flux event
%input voltage into the halogen lamp array regulated by the Variac
%several measurements are taken for each steady state event
%variac voltage at steady state (read with true RMS multimeter)
Vin=[40.5 50.7 60.87 70.68 80.56 90.5;40.5 50.7 60.87 70.68 80.56 90.5;40.5 50.7 60.87 70.68 80.56 90.5];  %Volts
%the input voltages are averaged together for each of the 6 events shown in this code
Vin_1=mean(Vin); %Average steady state input volts
%% steady state calculations ---------------------------------------------------------------------------------------
num_samples=120; %average steady-state data over 120 seconds (sampling rate = 1 Hz)
for i=1:length(ss)
   PHFS_V1_1(i)=mean(PHFS_V1(ss(i)-num_samples:ss(i)));
end
%% data processing ----------------------------------------------------------------------------------------------------%%
PHFSV1=PHFS_V1_1.*10^6; %convert PHFS mean voltage to microVolts
%heat flux fifth order fit equation coefficients determined from system
%calibration using SB gage
p=[-.0000000029267, .0000011894, -.00017949, .012841, -.41415, 5.4372];
HF_abs_1=eg.*polyval(p,v1); %absorbed heat flux in PHFS, W/cm^2
%Method 1
S1=V1./HF_abs_1; %PHFS sensitivity, microV/W/cm^2
S1a=mean(S1) %reported PHFS sensitivity, microV/W/cm^2
%% plots ----------------------------------------------------------------------------------------------------
```

```
%PHFS sensor voltage vs time without voltage bias
figure(1)
plot(time,PHFS_V1, 'k-', 'linewidth', 1);
xlabel('Time, {\itt} (s)','FontSize',10,'FontName','Helvetica','FontWeight','bold')
ylabel('PHFS Voltage, {\itV}_{t} (V)','FontSize',10,'FontName','Helvetica','FontWeight','bold')
%PHFS sensor voltage vs Absorbed Heat Flux
figure(2)
plot(HF_abs_1,PHFS_V1_1,'r','linewidth',2);
plot(0,0)
xlabel('Net Absorbed HF (W/cm^2)')
ylabel('Voltage(uV)')
title('PHFS Voltage vs. Absorbed Heat Flux')
%PHFS sensor sensitivity vs Absorbed Heat Flux
figure(3)
title('Sensitivities vs. Heat Flux')
plot(HF_abs_1,S1,'xr','markersize',5,'Linewidth',3)
xlabel('Net Absorbed HF (W/cm^2)')
ylabel('Gage Sensitivity (micro-Volt/(W/m{^2}))')
```